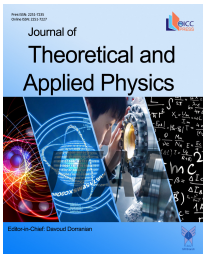

Volume 19, Issue 5, 192548 (1-23)

Journal of Theoretical and Applied Physics (JTAP)

https://doi.org/10.57647/j.jtap.2025.1905.48

Investigation of D-Glutamine dimer: Characterization of N—H···O bond using experimental - IR, Raman, UV-Vis, ECD spectroscopy techniques, supported by computational - MD, DFT, NBO, AIM, NCI methods

Mithil Kotyagol, J. Tonannavar, Jayashree Tonannavar*

Vibrational Spectroscopy Group/Molecular Modelling Laboratory, Department of Physics, Karnatak University, Dharwad, India.

***Corresponding author:** jjtonannavar@kud.ac.in

Original Research

Received:
19 May 2025
Revised:
28 August 2025
Accepted:
4 September 2025
Published online:
31 October 2025

Abstract:

The zwitterionic *inter*- molecular N—H···O bonded dimer structure was proposed for D-Glutamine. The identification of *inter*- molecular N—H···O bond was aided by reported XRD and IR absorption spectral features. We obtained *inter*- molecular N—H···O bonded dimer, trimer, and tetramer species during molecular dynamics simulation. We selected the dimers with the longest maximum residence time for DFT calculations and labeled them as D-I, D-II, D-III, and D-IV for our reference. We determined the H-bond correlation for these dimers at the B3LYP/6-31G(d,p) level. D-I has the shortest H···O distance, a greater change in N—H bond length between bonded and free bond length, a larger decrease in N—H stretching frequencies when it's bonded, higher stabilization energy from NBO analysis, and more H-bond interaction energy from AIM analysis. Therefore, D-I was selected for further detailed study. D-I satisfactorily with the reported XRD structure of D-Glutamine. D-I aligns well with the experimental IR and Raman spectral features. We studied excited electronic transitions using UV-Visible and Electronic Circular Dichroism spectral measurements. D-I was further electronically characterized using NBO, MEP, HOMO-LUMO, AIM, and NCI analysis. With all these characterizations, the D-I was in excellent agreement with the experimental spectral measurements.

Keywords: D-Glutamine; Molecular dynamics simulation; Density functional theory; N—H···O bond; ECD spectrum

1. Introduction

As the building blocks of proteins in living organisms, amino acids (AAs) are the most important chiral biomolecules [1]. The non-proteinogenic forms of AAs, D-AAs, and their amide derivatives are known to play a significant role in the formation of bacterial cell walls and antibiotics. D-Glutamine and D-Glutamic acid amides are essential for oxidative stress, nitrogen metabolism, and mitochondrial action. As a result, they are crucial raw materials used in the manufacture of food additives and pharmaceutical products [2]. In this paper, we referred to D-Glutamine as D-Gln for short. The neutral molecular structure of D-Gln is shown in figure 1. D-Gln is the stereoisomer of L-Glutamine (L-Gln). The crystal structure of L-Gln was studied using the XRD technique [3]. L-Gln has a zwitterionic (ZW) form and is arranged in an orthorhombic unit cell with a space group of $P2_12_12_1$, where the cell dimensions are $a = 16$ Å, $b = 7.76$ Å, and $c = 5.10$ Å. Each unit cell contains four molecules. The N—H···O bond forms between all five hydrogen atoms of the amine and ammonium group, which extend in three dimensions to form the crystal. The crystal structure was further studied using neutron diffraction; these results are consistent with the reported XRD structure [4]. Pawlukojc et al. used inelastic neutron scattering (INS), IR, Raman, and DFT techniques to study the vibrational monomer structure of L-Gln [5]. They studied in three different frequency regions, namely the high-frequency region ($3400 - 1500$ cm^{-1}). The IR spectra show a strong continuum absorption band, spread from 2900 cm^{-1} up to 2400 cm^{-1}, indicating the existence of strong N—H···O bonding in L-Gln. Torsional and bending bands caused by NH_3^+, NH_2, and CH_2 are observed in the medium-frequency range ($1500 - 600$ cm^{-1}). In the far-

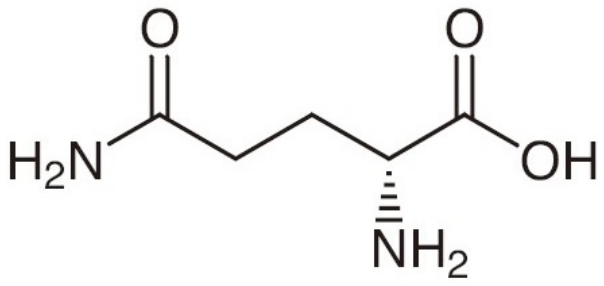

Figure 1. Neutral molecular structure of D-Glutamine.

infrared region (below 600 cm^{-1}), torsional and bending skeleton deformations of L-Gln were discussed. Bands due to COO^- and NH_3^+ showed L-Gln's ZW monomer structure. N. H. Rhys et al. studied the hydrogen bonding (H-bonding) ability of L-Gln using the empirical potential for structure refinement simulation in an aqueous medium, in conjunction with neutron diffraction experiments [6]. These experiments examined interactions between Gln-water and Gln-Gln. Calculations of the coordination number and radial distribution function (RDF) supported the observation that the Gln-Gln interaction predominates over the Gln-water interaction. For their reference, they partitioned the monomer structure into two parts: the backbone ($B:COO^-CHNH_3^+$) and the side chain ($S:CH_2CH_2CONH_2$). This suggests that the backbone of the D-Gln molecule exhibits greater coordination with water molecules as compared to its side chain. Because the charged groups on the backbone of D-Gln molecule attract water more effectively than the dipole of its side chain. They also found that both carboxyl and carbonyl groups interact more readily with water molecules than the amine groups. Additionally, this study reported four types of N—H$\cdots$O bonded interactions: NH_3^+ with COO^- [backbone-backbone (B-B)], NH_2 with COO^- [sidechain-backbone (S-B)], NH_3^+ with CO [backbone-sidechain (B-S)], and NH_2 with CO sidechain-sidechain (S-S). Quantifying L- and D-amino acids in enantiomeric mixtures using Electronic Circular Dichroism (ECD) spectroscopy. This method utilized a standard calibration curve, combining the techniques of circular dichroism and achiral liquid chromatography. They reported concentration-dependent ECD spectra for enantiomeric mixtures of AAs [7]. Previous studies have reported the existence of H-bonding and various N—H$\cdots$O bonded dimer structures for L-Gln. However, to the best of our knowledge, no other group has reported the structural, vibrational, electronic characterization and excited electronic transitions of the N—H$\cdots$O bonded dimer of D-Gln. In this study, we have characterized the N—H$\cdots$O bonded dimers forms using the B3LYP/6-31G(d,p) method with the SCRF-SMD solvation approach for D-Gln, supported by Molecular Dynamics (MD) simulations, Density Functional Theory (DFT) calculations, Natural Bond Orbital (NBO), Molecular Electrostatic Potential surface (MEP), Highest Occupied Molecular Orbital (HOMO) and the Lowest Unoccupied Molecular Orbital (LUMO), Atoms In Molecules (AIM), and Non-Covalent Interactions (NCI) analyses along with experimental measurements from the IR, Raman, UV-visible (UV-Vis), and ECD spectra.

2. Material and methods

We purchased D-Gln from *Sigma Aldrich* Chemicals, Bangalore, which has the molecular formula $C_5H_{10}N_2O_3$, colourless compound and a molecular weight of 146.14 g/mol. We used D-Gln for our experimental FT-IR, FT-Raman, UV-Vis, and ECD spectral measurements without doing any further purification.

2.1 Experimental techniques

We measured the FT-IR spectrum for D-Gln, in the wavenumber range from 4000 to 400 cm^{-1}, using a ThermoFisher *Nicolet-6700* instrument equipped with an Alum standard ETC Ever-Glo IR source, KBr beam splitter, and DTGS detector. We prepared the sample by mixing the D-Gln sample with dry KBr in a ratio of 1:100, pelleting it, and then placing it in the spectrometer. Spectral signals were collected at a resolution of 4 cm^{-1} for 100 scans. The FT-Raman spectrum was recorded using the BRUKER *RFS 27* MultiRAM, a standalone FT-Raman spectrometer capable of scanning range from 4000 to 50 cm^{-1}. The system is equipped with an Nd-YAG laser source emitting at a wavelength of 1064 nm and a liquid nitrogen-cooled Germanium diode detector. The scattered light was collected at 180° using a high-throughput lens. Spectral data were recorded at a resolution of 4 cm^{-1} for 500 scans. The ECD spectrum was measured using a *Jasco-1500* Circular Dichroism spectrophotometer in the wavelength range of $190-750$ nm. The instrument consists of an Xe arc lamp as the light source with nitrogen purging, an energy-discrimination double-prism monochromator, and a photomultiplier tube (PMT) detector. Distilled water was used as the solvent for preparing the sample; samples were placed in a quartz cell cuvette with a path length of 1 mm. Spectral data were collected at a scanning speed of 100 nm/min with a bandwidth of 1 nm. The UV-visible spectrum was recorded using a *Jasco V-670* double-beam spectrophotometer equipped with a Czerny-Turner mount in the wavelength range of $200-750$ nm. The instrument features a deuterium lamp source and PMT detector. Samples were prepared using distilled water and placed in quartz cells with a path length of 10 mm. Background absorbance caused by air was subtracted, and the spectrum was baseline-corrected. Data were collected at a scanning speed of 100 nm/min with a bandwidth of 1 nm.

2.2 Computational techniques

2.2.1 SCRF- DFT and TD-DFT calculation

We performed geometrical optimization, vibrational frequency calculation, and excited electronic transitions using the *Gaussian 09W* program package at the B3LYP/6-31G(d,p) level [8]. For visualization, we used the *GaussView 5W* software program [9]. We carried out vibrational assignments using the Vibrational Energy Distribution Assignment (VEDA) 4.0 program to calculate Potential Energy Distributions (PED) values [10]. NBO analysis was performed using NBO Version 3.1 implemented in the *Gaussian 09W* package at the B3LYP/6-31G(d,p) level. The *Gaussian* output.*wfn* file is used as input for the *Multiwfn* program to perform AIM and NCI analyses. The first step is to determine a stable ZW monomer and using this monomer

to find the most stable ZW dimer for characterization in terms of structural, vibrational, and electronic properties. To obtain a stable conformer, we performed potential energy surface (PES) scan for the neutral (NE) monomer structure of D-Gln at the RHF/6-31G level. We scanned all the angles, which are responsible for the non-rigidity of the molecule [11, 12]. Initially, we scanned the dihedral angle τ_1 (8C-2C-1C-3C), and obtained the minimum energy structure *M1*. Using *M1* structure PES scan was performed for the COOH moiety dihedral angle τ_2 (1C-2C-8C-15O), which yielded the minimum energy *M2* structure. Further, considering the *M2* structure, we scanned the dihedral angle τ_3 of the OH group (16H-14O-8C-2C), yielding the minimum energy *M3* structure. We performed all these previous scans by varying the dihedral angles, which ranged from -180° to 180° with a 10° increment. For the *M3* structure, we scanned the NH_2 moiety (near COOH) dihedral angle τ_4 (13H-7N-2C-1C), and obtained the same minimum energy structure as the previous *M3* structure. Similarly, we scanned the NH_2 moiety (near C=O) and dihedral angle τ_5 (19H-18N-9C-3C), and obtained the same *M3* structure. Both NH_2 moieties are scanned by varying angles ranging from 0° to 180° with a 10° increment. All PES scans are shown in figure 2. In the XRD paper and vibrational analysis of monomer structure, it was shown that Gln exists in the ZW form. In the *Gaussian 09W*, D-Gln exists in a neutral structure in the gas phase. Therefore, we optimized the structure at B3LYP/6-311G++(d,p) with SCRF implicit solvation using water as the solvent, resulting in the ZW structure, which we denoted as M_{ZW} [13]. The optimized ZW structure M_{ZW} of D-Gln is as shown in figure 3. Similar to N. H. Rhys et al, for our reference, we also partitioned this structure into two parts: backbone (B:$COO^-CHNH_3^+$) shown by the dotted circle and the side chain (S:$CH_2CH_2CONH_2$) shown by solid circle, [6]. This optimized M_{ZW} was used as the input structure for the MD simulation.

2.2.2 Molecular dynamical simulation

We used *Gromacs* 5.1.1 software for classical MD simulation, employing the all-atom optimized potential for liquid simulations (OPLS-AA) force field [14–17]. With a box size of $0.7 \times 0.4 \times 0.3$ nm, added 20 M_{ZW} (section 2.2.1). We used the TIP4P (transferable intermolecular potential 4P) water model for solvation, adding 1,000 water molecules. Partial atomic charges for the M_{ZW} were calculated using CHELPG (Charges from Electrostatic Potentials Using a Grid) in *Gaussian 09W* and are given in Table 1 [18]. The Lennard-Jones potential parameters for M_{ZW} were obtained from the *Gromacs* library and given in Table 2 [19]. To prevent steric conflicts during MD simulations, an initial energy minimization step was performed using a steepest descent integrator with a step size of 0.01. Subsequently, the system was heated using a Velocity-Rescale thermostat with a time constant of 0.1 ps to maintain a constant temperature of 300 K, and a Parrinello-Rahman barostat with time constant of 2 ps was applied to maintain a constant pressure of 1 bar. After equilibration, MD production was performed for 1 ns using the Parrinello-Rahman barostat and Nose-Hoover thermostat at a time step of 200 fs, employing the leap-frog algorithm for integrating the equation of motion. The LINear Constraint Solver for Molecular Simulation (*LINCS*) algorithm was employed to impose restrictions on atoms involved in covalent and hydrogen bonds (H-bonds) [20]. Short-range electrostatic interactions were computed using the Particle Mesh Ewald (PME) Method, with a charge grid spacing of 1 nm [21]. To minimize edge effects and correct for dispersion, all simulations were conducted with periodic boundary conditions (PBC) in three dimensions.

3. Results and discussion

3.1 MD analysis

All MD analyses were conducted after production runs, indicating the presence of *inter*-molecular N—H$\cdots$O bonded oligomers, including non-closed dimers, closed dimers, trimers, and tetramers species were observed throughout the simulation. Figure 4 presents a snapshot of these oligomers during the simulation at 560 ps timeframe. We calculated maximum residence time (MRT) values for all oligomers. For each interaction from the non-closed dimer group, the dimers with the greater MRT values, B-B (180 ps), S-B (170 ps), B-S (160 ps), and S-S (100 ps) for our reference, we denoted as these dimers as D-I, D-II, D-III, and D-IV, respectively (see Table 3). These dimers having high MRT values compared to closed dimers, trimers, and tetramers species. Therefore, we considered D-I, D-II, D-III, and D-IV for further DFT analysis. MRT values for the closed dimer, trimer, and tetramer species are given in Table 4, Table 5, and Table 6, respectively. Additionally, average lifetime values for all possible N—H$\cdots$O bonds are given in Table 7. The N—H$\cdots$O bonds were characterized using radial distribution function (RDF) analysis [$g(r)$, also known as pair distribution function]. The RDF represents the probability of finding a donor atom A and acceptor atom B [$g_{AB}(r)$] within a distance range dr from r to $r+dr$. As $dr \to 0$, the number density of B atoms within a spherical shell of volume $4\pi r^2 dr \bullet g_{AB}(r)$ surrounding atom A yields the probability distribution [22, 23]. RDF plots of $g_{\mathrm{H}\cdots\mathrm{O}}$ for Gln-Gln interactions, including B-B, B-S, S-B, and S-S, and Gln-water interactions are shown in figure 5, and corresponding first-shell maxima (r_{max}) values are given in Table 8. The RDF plot indicates that the B-B interaction has a shorter r_{max} value of 1.68 Å, compared to S-B (1.77 Å), B-S (1.99 Å), and S-S (2.18 Å), suggesting B-B interaction was stronger. Similarly, considering the Gln-water interaction r_{max} values, the COO^- with water (1.70 Å) and CO with water (1.71 Å). NH_3^+ with water (1.87 Å) and NH_2 with water (1.87 Å). The r_{max} values indicate that the CO groups interaction with water is stronger as compared to the NH groups interaction with water. RDF r_{max} values indicate that among Gln-Gln and Gln-water interactions, Gln-Gln was found to be stronger. Our MD results are consistent with the reported work by N. H. Rhys et al. [6].

3.2 Correlations of H-bond descriptors

We performed optimization, computed the vibrational frequencies, NBO and AIM analysis for dimers D-I to D-IV (section 3.1) at the B3LYP/6-31G(d,p) level, and the optimized structures are shown in figure 6. In this section,

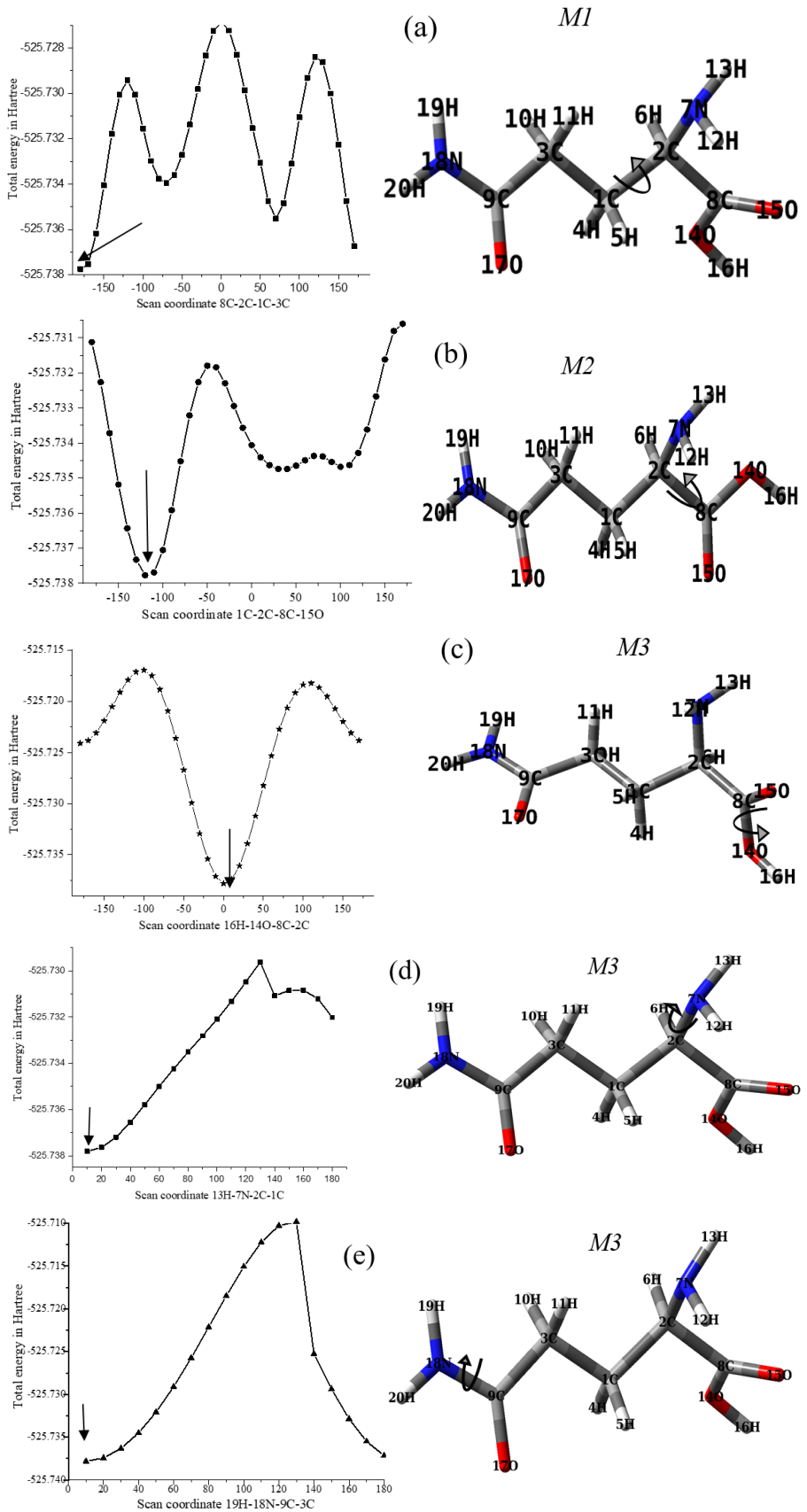

Figure 2. Potential energy surface scan for neutral D-Glutamine structure at RHF/6-31G. For the dihedral angles (a) τ_1 = 8C-2C-1C-3C, (b) τ_2 = 1C-2C-8C-15O, (c) τ_3 = 16H-14O-8C-2C, (d) τ_4 = 13H-7N-2C-1C and (e) τ_5 = 19H-18N-9C-3C (marked with arrow on the left panel) corresponding lowest energy monomer structures *M1*, *M2*, and *M3* (shown on the right panel) respectively.

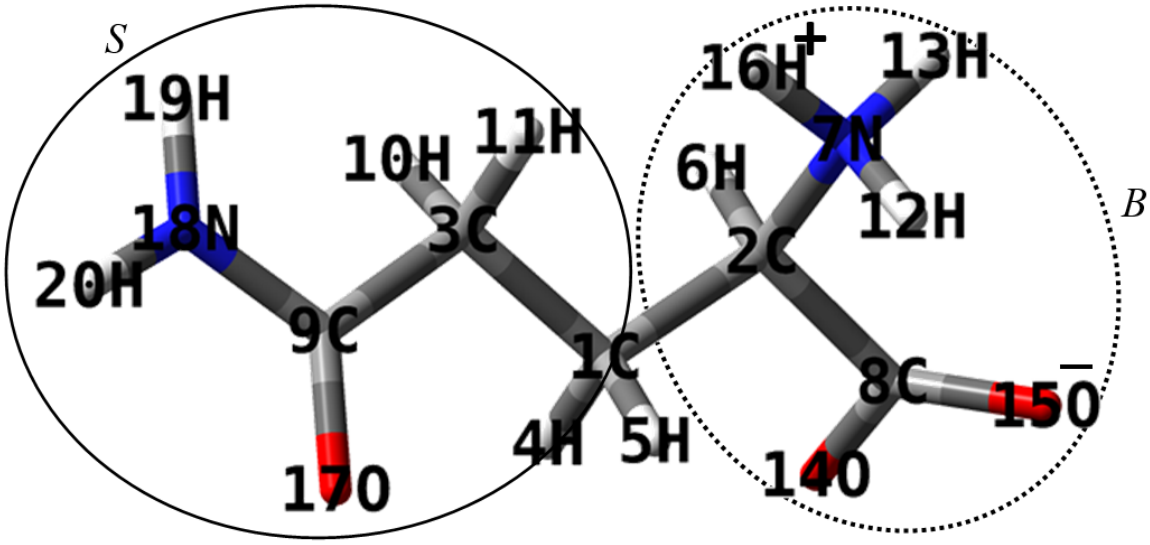

Figure 3. Optimized zwitterionic monomer structure (M_{ZW}) of D-Glutamine at B3LYP/6-31G++(d,p) level with atom numbering. [solid circle represents side chain (S: $CH_2CH_2CONH_2$) and dotted circle represents backbone (B: $COO^-CHNH_3^+$)].

Table 1. Partial atomic charges of D-Glutamine monomer, calculated at B3LYP/6-311++G(d,p) method using CHELPG charges.

Atom	ESP Charges	Atom	ESP Charges
C1	0.023277	H11	0.072928
C2	0.220659	H12	0.366520
C3	−0.247346	H13	0.338274
H4	0.012129	O14	−0.866138
H5	0.021067	O15	−0.848099
H6	0.048151	H16	0.381645
N7	−0.489496	O17	−0.801675
C8	0.828953	N18	−1.027831
C9	0.957238	H19	0.452077
H10	0.093753	H20	0.463915

Table 2. The Lennard-Jones potential parameters for D-Glutamine monomer.

Atom types	Atoms with numbering	OPLS Force field	$\sigma \times 10$ (nm)	$\varepsilon \times 10$ (kJ/mol)
CH (NH_3^+)	C2	293	3.50	2.76144
	H6	140	2.50	1.25520
COO^- carboxylate	C8	271	3.75	4.39320
	O14/O15	272	2.96	8.78640
NH_3^+	N7	287	3.25	7.11280
	H12/H13/H16	290	0.00	0.00000
alkane CH_2	C1, C3	136	2.96	8.78640
	H4/H5/H10/H11	140	2.50	1.25520
C=O in amide	C9	235	3.75	4.39320
	O17	236	2.96	8.78640
NH_2: primary amide	N18	237	3.25	7.11280
	H19/H20	140	2.50	1.25520

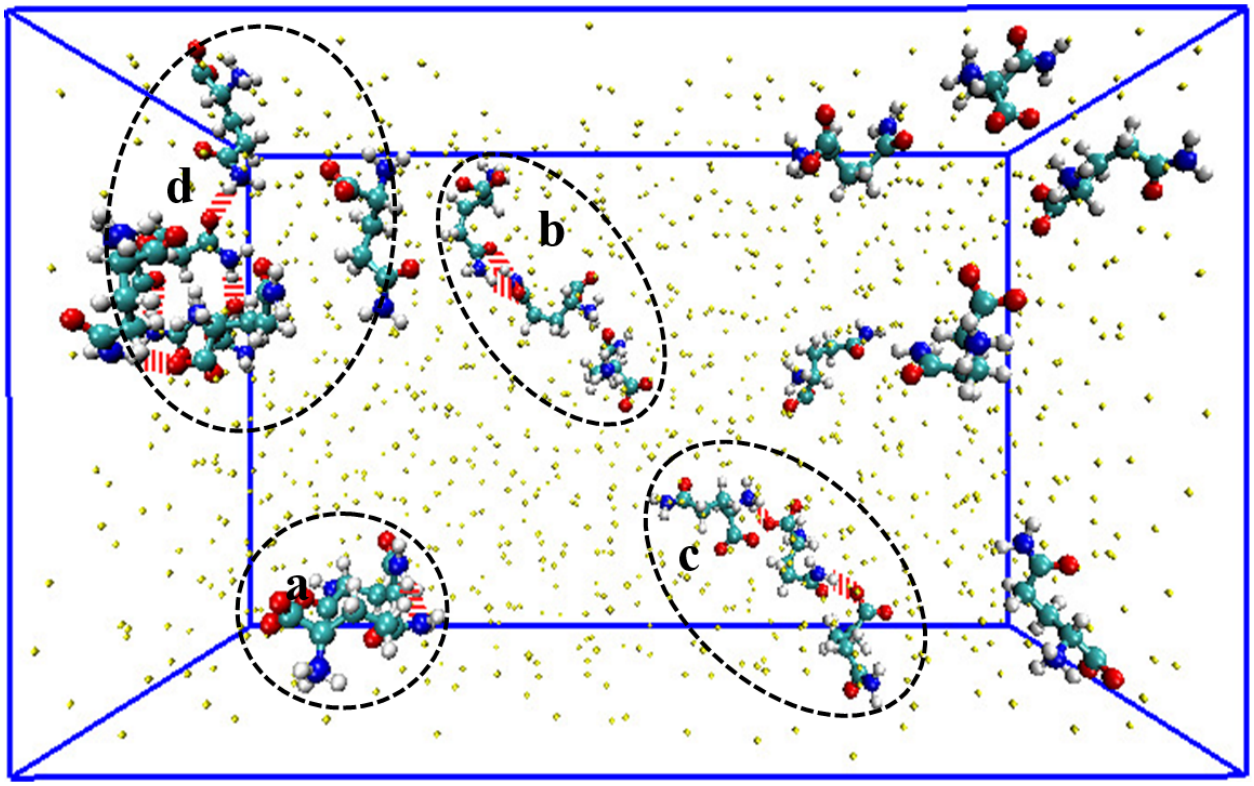

Figure 4. Snapshot of equilibrated simulation box containing Glutamine with water at 560ps. Glutamine is shown in ball and stick style, N—H···O bonds are represented by broken red lines, and water as dots. Dotted circles represent N—H···O bonded (a) non-closed dimer, (b) closed dimer, (c) trimer, and (d) tetramer formed during MD simulation.

Table 3. Maximum residence time (MRT) values of non-closed dimers of D-Glutamine.

Sl. No	Moieties	N—H···O bond	MRT (ps)
1	NH_3^+ & COO^- (B-B)	N27-H33···O15 (D-I)	180
2		N7-H16···O34	120
3		N7-H16···O35	120
4		N27-H33···O14	110
5		N7-H12···O35	70
6		N27-H32···O14	20
7	NH_2 & COO^- (S-B)	N18-H20···O34 (D-II)	170
8		N38-H40···O15	150
9		N38-H39···O15	110
10		N18-H19···O34	110
11	NH_3^+ CO (B-S)	N27-H33···O17 (D-III)	160
12		N7-H16···O37	70
13		N7-H12···O37	50
14	NH_2 CO (S-S)	N18-H20···O37 (D-IV)	100
15		N38-H39···O17	90

Note: B-Backbone, S-Sidechain.

Table 4. Maximum residence time (MRT) values of closed dimers of D-Glutamine.

Closed dimers	MRT (ps)
N27-H33···O17 & N18-H20···O34	50
N7-H16···O35 & N27-H32···O14	20
N7-H16···O34 & N7-H16···O35	30
N7-H16···O35 & N7-H12···O35	10
N7-H12···O35 & N7-H16···O34	10
N27-H33···O17 & N7-H12···O35	10
N18-H19···O34 & N18-H19···O34	30
N18-H19···O34 & N38-H39···O15	40
N18-H20···O37 & N18-H20···O37	30
N18-H20···O37 & N18-H19···O34	20
N18-H19···O34 & N18-H20···O37	10
N7-H16···O37 & N18-H20···O34	10
N18-H19···O34& N10-H20···O3	30
N38-H39···O15 & N7-H16···O34	20
N18-H20···O34 & N7-H12···O37	20
N7-H16···O37 & N38-H39···O15	10
N27-H33···O17 & N38-H39···O15	30
N38-H39···O15 & N7-H16···O37	10
N18-H20···O34 & N7-H12···O37	20

Table 5. Maximum residence time (MRT) values of trimers of D-Glutamine..

Trimers	MRT (ps)
N58-H59···O37 & N38-H39···O14	40
N7-H16···O34 & N27-H32···O55	30
N27-H33···O14 & N27-H32···O56	20
N18-H19···O34 & N38-H39···O56	30
N38-H39···O14 & N47-H52···O17	10
N7-H12···O35 & N58-H60···O37	10
N27-H33···O14 & N38-H39···O56	10
N7-H16···O35 & N38-H40···O57	10
N18-H19···O34 & N7-H12···O56	10
N7-H16···O34 & N38-H39···O56	10
N7-H16···O37 & N38-H19···O55	10
N7-H16···O34 & N38-H39···O56	10
N27-H33···O14 & N7-H16···O56	10
N7-H12 ···O35 & N18-H20 ···O35	20

Table 6. Maximum residence time (MRT) values of Tetramers of D-Glutamine.

Tetramers	MRT (ps)
N38-H39···O14, N7-H12···O56, N47-H52···O76	10
N38-H39···O14, N27-H32···O56, N58-H59···O76	10
N7-H12···O35, N27-H34···O55, N58-H59···O75	10
N27-H33···O14, N7-H16···O34 & N58-H59···O55, N58-H59···O76	10
N38-H39···O15 & N18-H19···O55, N47-H54···O75, N58-H60···O15	10
N38-H39···O15, N27-H34···O55, N47-H52···O75	10

Table 7. Average N—H···O bonds lifetime value in picoseconds for D-Glutamine.

Sl. No.	Moieties	N—H···O bonding	Lifetime in ps
1.	NH_3^+ & COO^- (B-B)	N27-H33···O15	30.75
2.		N7-H16···O34	11.81
3.		N7-H16···O35	14.62
4.		N27-H33···O14	10.56
5.		N7-H12···O35	09.78
6.		N27-H32···O14	10.00
7.	NH_2 & COO^- (S-B)	N18-H20···O34	32.06
8.		N38-H40···O15	45.00
9.		N38-H39···O15	18.75
10.		N18-H19···O34	32.86
11.	NH_2 & CO (S-S)	N18-H20···O37	49.00
12.		N38-H39···O17	17.00
13.	NH_3^+ & CO (B-S)	N27-H33···O17	28.85
14.		N7-H16···O37	21.00
15.		N7-H12···O37	13.26

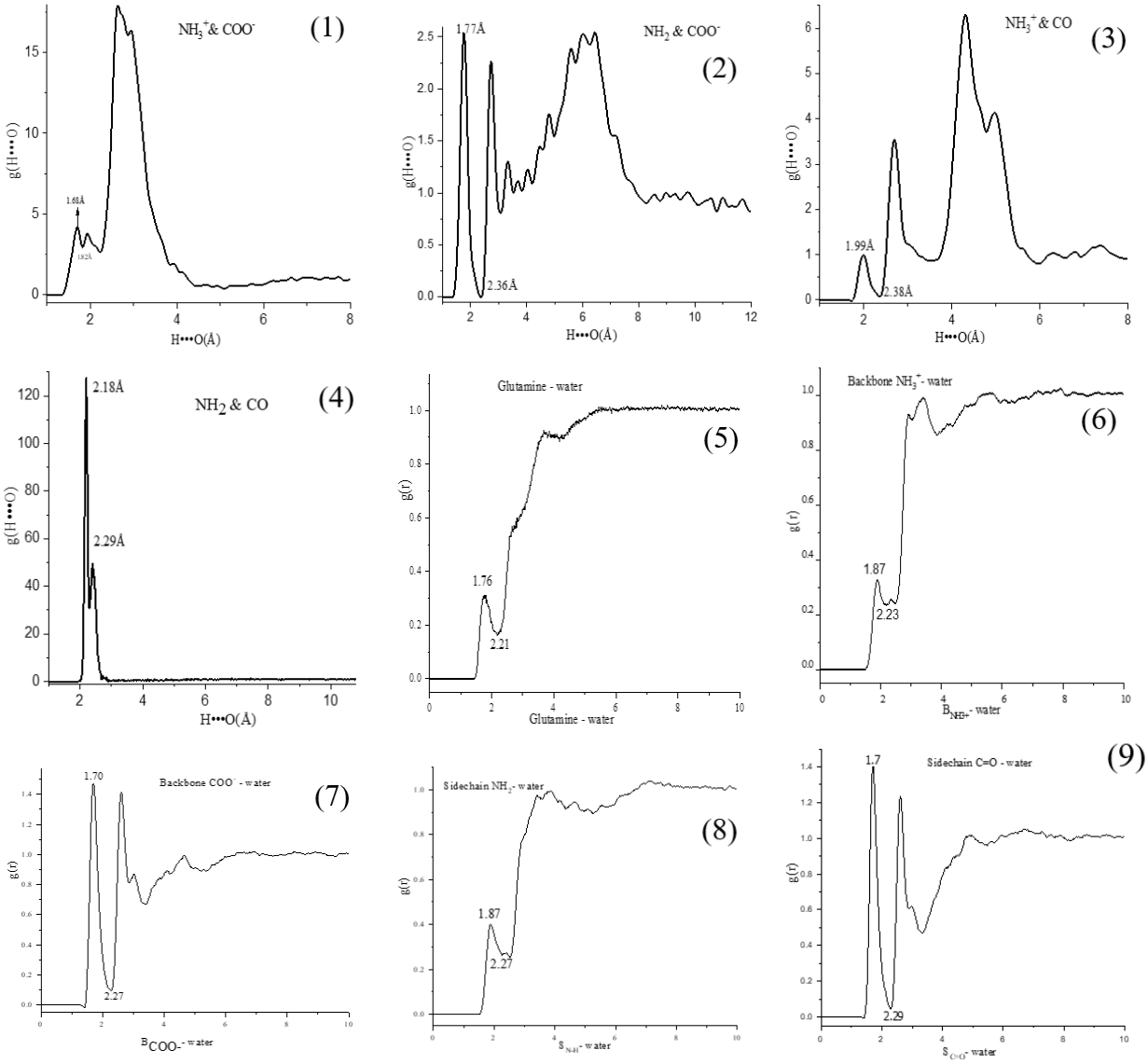

Figure 5. RDF plots of different interactions, (1) NH_3^+ with COO^-, (2) NH_2 with COO^-, (3) NH_3^+ with CO, (4) NH_2 with CO, (5) Glutamine - water, (6) NH_3^+ with water, (7) COO^- with water (8) NH_2 with water, (9) CO with water.

Table 8. Radial distribution function (RDF) values for different moieties interactions of D-Glutamine.

Interactions	Moieties	RDF 1st peak (Å)
Glutamine with Glutamine	NH_3^+&COO^- (B-B)	1.68
	NH_2&COO^- (S-B)	1.77
	NH_3^+&CO (B-S)	1.99
	NH_2&CO (S-S)	2.18
Glutamine with water	COO^- - water	1.70
	CO - water	1.71
	NH_3^+ - water	1.87
	NH_2 - water	1.87

Note: B- Backbone, S-Sidechain.

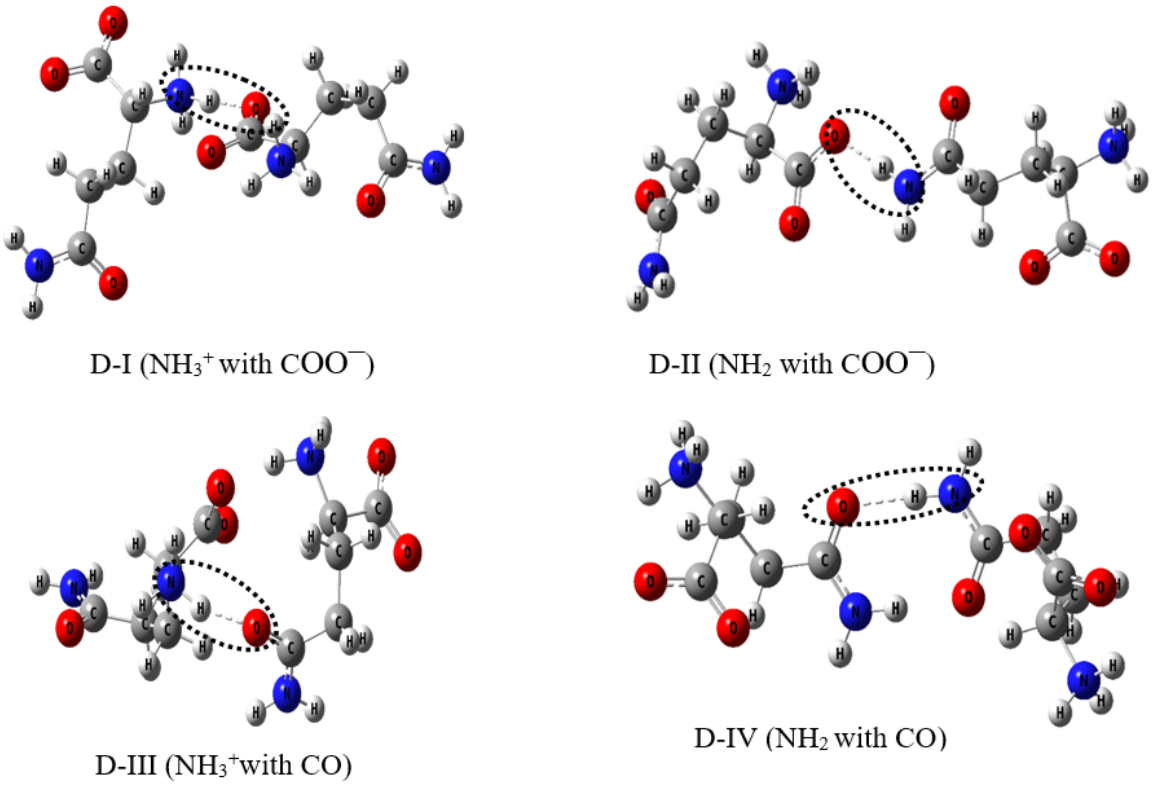

Figure 6. Optimized zwitterionic D-I, D-II, D-III, and D-IV structures at B3LYP/6-31G(d,p) level of D-Glutamine. The N—H···O bonding moieties are encircled with the dotted line.

we are discussing correlations of H-bond descriptors for dimers D-I to D-IV, which are shown in figure 7, and the parameters are given in Table 9 [11]. Optimized geometric properties such as H-bond lengths H···O distance for D-I (1.65 Å), D-II (1.72 Å), D-III (1.83 Å), and D-IV (1.88 Å) (detailed discussion in section 3.3). Here, D-I shows a minimum H···O distance, and N—H···O bond angle for D-I is 179.9° which means it is more linear. In figure 7a, we are discussing how the change in N—H bond length (ΔN—H = free N—H bond length - bonded N—H bond length) varies with respect to the H···O distance. As the H···O distance increases, the ΔN—H decreases from D-I to D-IV. With a shorter H···O distance, D-I showed a greater ΔN—H value. The ΔN—H with respect to H···O distance abruptly decreases from D-I to D-II. ΔN—H gradually decreases from D-II to D-III, and likewise from D-III to D-IV. In figure 7b, we are discussing how the frequency shift ($\Delta\bar{\nu}$ = free N—H stretching frequency - bonded N—H stretching frequency) varies with respect to ΔN—H (detailed discussion in section 3.4). There is a linear relationship between different species. We observed a maximum frequency shift for D-I in relation to a greater ΔN—H value. There is a sharp decrease in $\Delta\bar{\nu}$ from D-I to D-II, similar to ΔN—H with H···O distance. The slow rate of change in $\Delta\bar{\nu}$ with re-

spect to ΔN—H was observed from D-II to D-III and from D-III to D-IV. D-I showed 710 cm^{-1} (21% redshift) $\Delta\bar{\nu}$, indicating strong N—H···O bonding. In figure 7c, we are discussing how the stabilization energy [$E^{(2)}$] varies with the corresponding H···O distance (detailed discussion in section 3.6.1). As the H···O distance increases, the $E^{(2)}$ decreases. D-I showed the highest $E^{(2)}$ value with a shorter H···O distance. The $E^{(2)}$ with respect to H···O distance suddenly decreases from D-I to D-II. $E^{(2)}$ changes slowly from D-II to D-III, and likewise from D-III to D-IV. D-I showed $E^{(2)}$ value of 33.5 kcal/mol, twice that of all other interactions, along with greater orbital overlapping, indicating strong N—H···O bonding. In figure 7d, we are discussing how the H-bond interaction energy (E_{HB}) varies with the corresponding H···O distance (detailed discussion in section 3.6.4). As the H···O distance increases, E_{HB} decreases. With a shorter H···O distance, D-I showed a −14.7 kcal/mol E_{HB} value, which is more than others. The E_{HB} with respect to H···O distance decreases from D-I to D-II. The E_{HB} slowly changes from D-II to D-III and from D-III to D-IV. From all correlations, it is clear that D-I has stronger N—H···O bonding than other dimers. These findings support the conclusions drawn by N. H. Rhys et al., indicating that the B-B (D-I) interaction is greater than other interactions [6]. Therefore, we considered the dimer D-I for further detailed discussion.

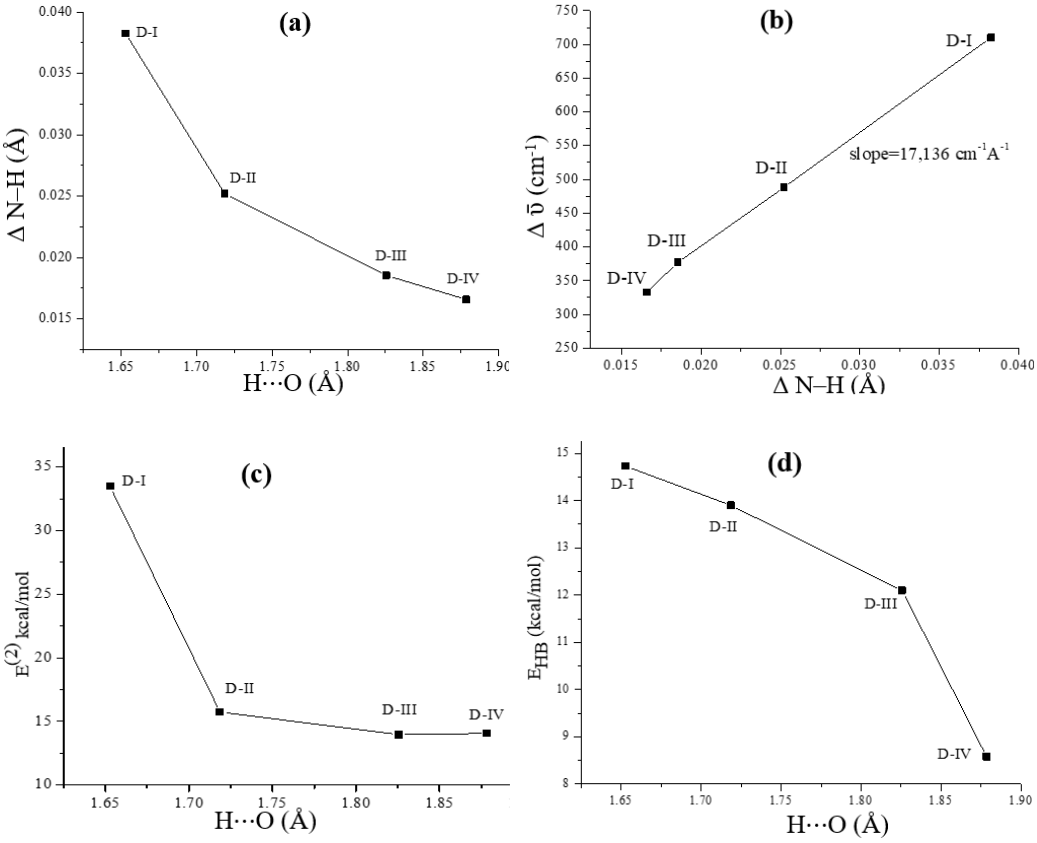

Figure 7. Correlation between H-bond descriptors of D-I (B-B), D-II (S-B), D-III (B-S), D-IV(S-S) a) ΔN—H with H···O, b) $\Delta\bar{\nu}$ with ΔN—H, c) stabilization energy ($E^{(2)}$) with H···O, d) H-bond interaction energy (E_{HB}) with H···O.

Table 9. Optimized geometric, vibrational, NBO and AIM parameters compared as H-bonding descriptors of D-Glutamine dimers.

Dimers	Moieties		H···O (Å)	∠N—H···O	d_1	d_2	ΔN—H	$\bar{\nu}_1$	$\bar{\nu}_2$	$\Delta\bar{\nu}$	$E^{(2)}$	E_{HB}
	Donar	Acceptor										
D-I	NH_3^+	COO^-	1.65	179.9	1.064	1.026	0.038	3363	2653	710	33.5	-14.7
D-II	NH_2	COO^-	1.72	161.7	1.050	1.025	0.025	3389	2901	488	15.7	-13.9
D-III	NH_3^+	CO	1.83	178.4	1.030	1.012	0.019	3510	3133	377	13.9	-12.1
D-IV	NH_2	CO	1.88	176.7	1.027	1.011	0.017	3515	3182	333	14.1	-08.6

∠- N—H···O bond angle in (°), d_1 - Bonded N—H bond length in Å, d_2 - Free N—H bond length in Å, ΔN—H = d_1 - d_2, $\bar{\nu}_1$ - Free N—H stretching frequency in cm^{-1}, $\bar{\nu}_2$ - Bonded N—H stretching frequency in cm^{-1}, $\Delta\bar{\nu}$ = $\bar{\nu}_1$ - $\bar{\nu}_2$ in cm^{-1}, $E^{(2)}$ - Stabilization Energy in kcal/mol, and E_{HB}- H bond interaction energy in kcal/mol.

3.3 DFT analysis

The phase of D-Gln is primarily influenced by its dominant H-bonding, along with *intra-* and *inter-* molecular interactions. Figure 8 shows the optimized ZW structure of D-I at the B3LYP/6-31G(d,p) level with atom numbering used in optimization [24]. We compared the optimized geometrical parameters of D-I with the experimental neutron diffraction parameters of L-Gln; bond lengths are given in Table 10, and bond angles are given in Table 11 [4]. The comparison broadly supports the D-I structure with N—H···O bonding. To assess the performance of the computed parameters with respect to the XRD values, we used statistics, namely, mean absolute deviations (MAD) and root mean square error (RMS error) [25]. For bond length, the MAD value for D-I is 0.01 Å, and the RMS error value is 0.014 Å. Similarly, for the bond angles, the MAD value is 0.530 Å and the RMS error value is 0.680 Å. These results indicate D-I is more than satisfactory with the experimental structure. We also performed DFT-D3 calculations at B3LYP/6-31G(d,p) level. The optimized energy of N—H···O bonded dimer structure with and without DFT-D3 are practically the same.

3.4 Vibrational analysis

The vibrational assignments for the monomer structure of L-Gln were reported by Pawlukojc et al. [5]. In this section we are discussing N—H···O bonded D-I vibrational assignments, computed at the B3LYP/6-31G(d,p) level. Here we compared the experimental IR and Raman spectra with the computed dimer D-I spectrum, see figure 9 and figure 10, respectively. The vibrational frequency data, along with assignments and PED values, are given in Table 12 [26]. The vibrational IR broad intense bands in the region $3400-2500\ cm^{-1}$ are spectral evidence for the N—H···O bonding in D-I dimer species. The N···O bond length of N—H···O bond has been correlated to the amount of N—H frequency shift: For shorter N···O bond lengths, there is a larger down-shift in the N—H frequency. N···O bond length for D-I is 2.71 Å, which is much less than the sum of van der Waal radii of N and O atoms i.e., 3.070 Å; therefore, there is more down-shift in N—H stretching frequency [27]. From the spectra structure correlation, there is NH_3^+ bonded stretching frequency in the region of $3144-3030\ cm^{-1}$, but due to strong N—H···O bonding, more down-shift was observed [28–30]. We observed NH_3^+ bonded stretching frequency band at 2646 cm^{-1} and computed band at 2653 cm^{-1}. The free NH_3^+ stretching frequency is observed at 3363 cm^{-1}; therefore, there is a 21% frequency down-shift from free to bonded stretching frequency. We observed a combination band near 2045 cm^{-1}, due to the combination of 1585 cm^{-1} (NH_3^+) and 584 cm^{-1} (COO^-) bands. Similarly, we also performed vibrational frequency analysis with DFT-D3 calculations at B3LYP/6-31G(d,p) level. As for the vibrational frequencies ($3500-2000\ cm^{-1}$), the MAD for the two sets (with and without DFT-D3) are practically the same: for IR: 10 cm^{-1}/10 cm^{-1} and Raman: 9 cm^{-1}/8 cm^{-1}; the standard deviations for IR: 13 cm^{-1}/12 cm^{-1}; for Raman: 12 cm^{-1}/11 cm^{-1}. The same is true for the $2000-80\ cm^{-1}$. From these calculations, we conclude that with and without DFT-D3 are practically the same.

3.5 Electronic transitions analysis

We measured the ECD and UV-Vis spectrum of D-Gln in water solvent in the range of $190-700$ nm at 5 mM concentration. There is a strong ECD band at 202 nm ($\sim$ 6.14 eV) and the UV-Vis band at 209 nm ($\sim$ 5.93 eV). There is no experimental band beyond 205 nm. We computed the ECD

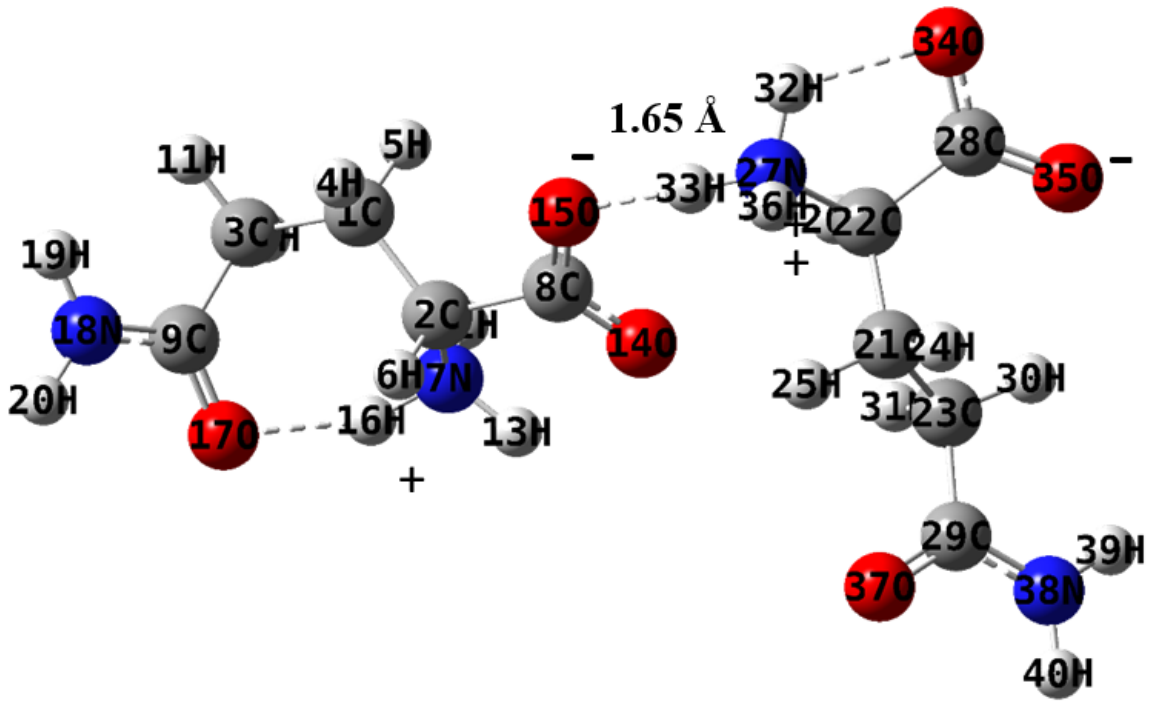

Figure 8. The optimized N—H···O bonded zwitterion dimer D-I structure of D-Glutamine at B3LYP/6-31G(d,p) level with atom numbering used in optimization.

Table 10. Optimized bond length parameter of N—H···O bonded dimer D-I at B3LYP/6-31G(d,p) of D-Glutamine along with experimental Neutron diffraction data.

Bond length	D-I (*Å*)	Expt[a] (*Å*)	Bond length	D-I (*Å*)	Expt[a] (*Å*)
C1-C2	1.536	1.545	C21-C22	1.536	1.528
C1-C3	1.555	1.532	C21-C23	1.537	1.523
C1-H4	1.093	1.093	C21-H24	1.097	1.110
C1-H5	1.095	1.101	C21-H25	1.096	1.105
C2-H6	1.095	1.096	C22-H26	1.096	1.097
C2-N7	1.513	1.496	C22-N27	1.514	1.498
C2-C8	1.537	1.536	C22-C28	1.546	1.540
C3-C9	1.514	1.516	C23-C29	1.281	1.262
C3-H10	1.096	1.096	C23-H30	1.092	1.104
C3-H11	1.093	1.101	C23-H31	1.100	1.100
N7-H12	1.026	1.04	N27-H32	1.034	1.044
N7-H13	1.028	1.022	N27-H33	1.064	1.027
N7-H16	1.045	1.045	N27-H34	1.025	1.048
C8-O14	1.281	1.260	C28-O34	1.293	1.240
C8-O15	1.291	1.238	C28-O35	1.281	1.262
C9-O17	1.281	1.253	C29-O37	1.271	1.231
C9-N18	1.341	1.331	C29-N38	1.351	1.334
N18-H19	1.045	1.045	N38-H39	1.010	1.004
N18-H20	1.014	1.009	N38-H40	1.011	1.010
intra- N7-H16···O17			*intra*- N27-H32···O35		
H16···O7	1.82	1.94	H32···O35	1.98	1.85
N7···O17	2.74	2.95	N27···O35	2.61	2.87
inter- N27-H33···O15			**MAD (*Å*)**	**RMS error(*Å*)**	
H33···O15	1.65	1.85	0.01	0.014	
N27···O15	2.72	2.87			

Note: Expt[a]- experimental neutron diffraction data of L-Gln [4], MAD -mean absolute deviations and RMS error - Root mean square error.

and UV-Vis spectrum for D-I using the TD-DFT method at the CAM-B3LYP/6-31G level with implicit solvation using water as a solvent; it yielded a band at 217 nm ($\sim$ 5.7 eV). We compared both experimental and computed bands, which are shown in figure 11. The band is assigned to the transition $^1A \leftarrow {}^1X$ (where X refers to the singlet ground state and A refers to the first singlet excited state). The electronic transition occurs from n(CO) $\rightarrow \pi^*$ (C=O on CO) groups [31]. The computed band is in fair agreement with the experimental ECD band value within 7% and UV-Vis band 4% deviation.

3.6 Electronic structure characterization

3.6.1 NBO analysis

NBO analysis was performed to study *intra-*/*inter-* molecular N—H···O bond interactions for D-I of D-Gln at the B3LYP/6-31G(d,p) level. This study facilitates the understanding of orbital interactions between donors and acceptors, as well as the formation of dimers. Stabilization energy for *intra-*/*inter-* molecular N—H···O bond interactions for D-I of D-Gln associated with each donor NBO (i) and acceptor NBO (j) are quantified by the second-order perturbative energy $E^{(2)}{}_{i\rightarrow j}$ and values are given in Table 13 [32–34]. Here, *inter-* molecular N—H···O bond showed

Table 11. Optimized bond angle parameter of N—H···O bonded dimer D-I at B3LYP/6-31G(d,p) of D-Glutamine compared with experimental Neutron diffraction data.

Bond angle	D-I(°)	Expt[a](°)	Bond angle	D-I(°)	Expt[a](°)
H6-C5-C1	109.8	109.7	H26-C25-C21	109.4	109.7
H6-C2-N7	105.1	106.6	H26-C22-N27	105.8	106.6
H6-C2-C8	107.3	108.7	H26-C22-C28	107.7	108.7
C1-C2-N7	111.5	111.1	C21-C22-N27	110.2	111.1
C1-C2-C8	114.1	112.3	C21-C22-C28	116.0	114.3
N7-C2-8	108.5	110.2	N27-C22-C28	107.4	109.2
C2-C1-C3	115.5	114.0	C22-C21-C23	112.9	114.0
C2-C1-H4	107.0	107.2	C22-C21-H24	109.7	107.2
C2-C1-H5	109.6	108.8	C22-C21-H25	108.4	108.8
C3-C1-H4	109.7	109.5	C23-C21-H24	110.4	109.5
C3-C1-H5	107.6	109.8	C23-C21-H25	107.9	109.8
H4-C1-H5	107.2	107.3	H24-C21-H25	107.4	107.3
C1-C3-C9	114.5	113.1	C21-C23-C29	112.3	113.1
C1-C3-H10	110.5	111.8	C21-C23-H30	110.7	111.8
C1-C3-H11	108.1	110.0	C21-C23-H31	108.8	110.0
C9-C3-H10	106.8	106.2	C29-C23-H30	110.5	108.9
C9-C3-H11	109.6	108.9	C29-C23-H31	107.2	106.2
H10-C3-H11	107.1	106.5	H30-C23-H31	107.1	106.5
C3-C9-O17	120.8	122.1	C23-C29-O37	122.1	122.1
C3-C9-N18	118.0	115.2	C23-C29-N38	116.3	115.2
O17-C7-N18	121.2	122.7	O37-C27-N38	121.6	122.7
C2-N7-H12	111.2	111.2	C22-N27-H32	105.5	107.3
C5-N7-H13	108.3	111.0	C25-N27-H33	110.9	111.0
C5-N7-H18	106.9	108.1	C25-N27-H38	110.9	108.1
H12-N7-H13	107.8	107.3	H32-N27-H33	112.1	111.2
H12-N7-H16	112.8	110.2	H32-N27-H34	108.1	110.2
H13-N7-H16	109.8	109.0	H33-N27-H34	109.2	109.0
C9-N18-H19	121.5	120.8	C29-N38-H39	121.6	120.8
C9-N18-H20	119.9	121.1	C29-N38-H40	119.8	121.1
H19-N18-H20	118.6	117.7	H39-N38-H40	118.6	117.7
C2-C8-O14	117.5	118.7	C22-C28-O34	118.1	118.7
C2-C8-O15	116.2	114.6	C22-C28-O35	116.2	114.6
O14-C8-O15	126.2	126.7	O34-C28-O35	125.7	126.7

Note: Expt[a]- experimental neutron diffraction data of L-Gln [4].

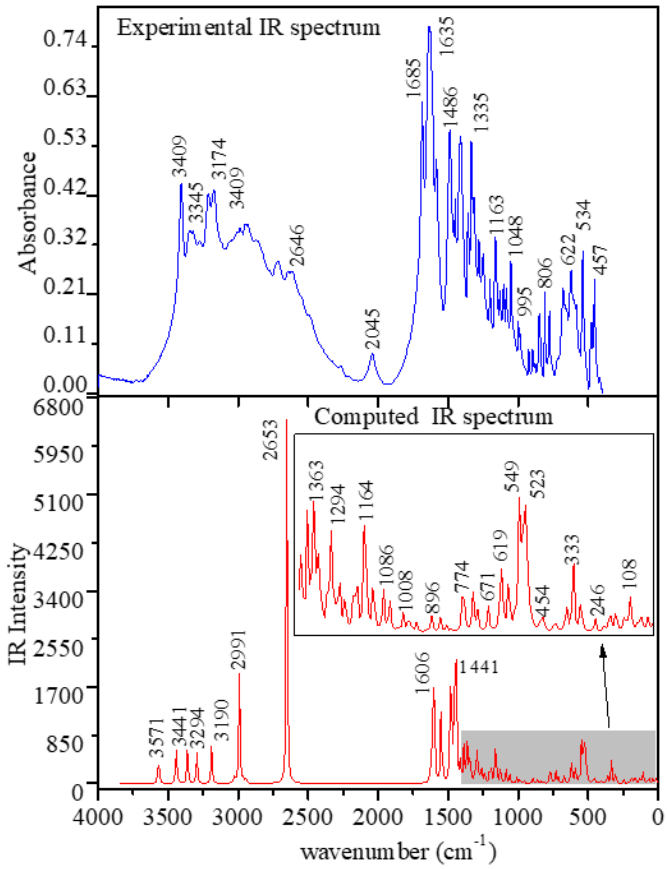

Figure 9. Experimental IR (top) and computed dimer D-I (bottom) IR spectra of D-Glutamine.

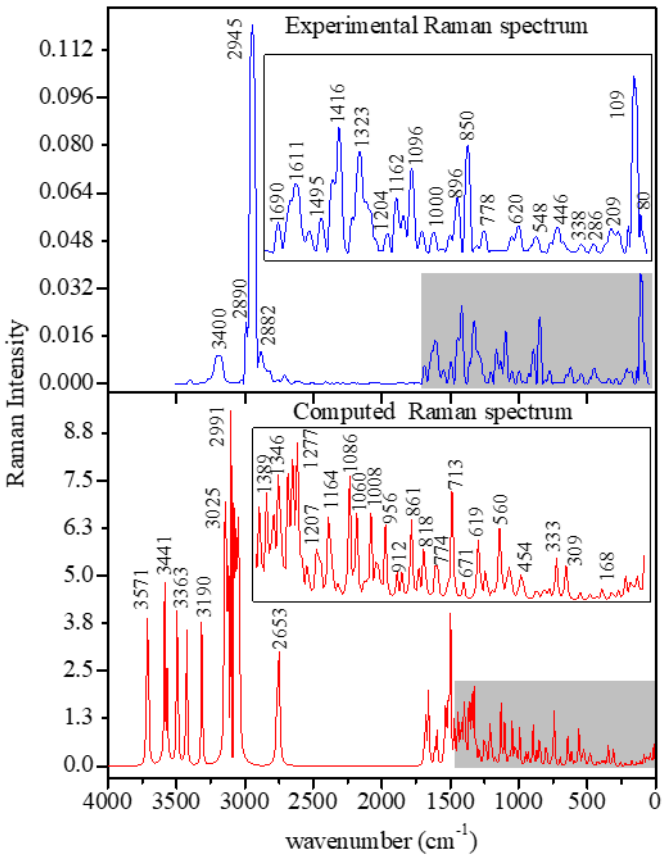

Figure 10. Experimental Raman (top) and computed dimer D-I Raman (bottom) spectra of D-Glutamine.

Table 12. Experimental and computed vibrational frequencies of D-I at the B3LYP/6-31G(d,p) level, with assignments for D-Glutamine. The percentage values of the potential energy distribution are given in square brackets.

wavenumber in cm^{-1}			D-I Intensity		Assignment
IR	Raman	D-I	IR	Raman	
-	-	3571	87	116	ν_{asym} NH_2 [100]
3409m	3400vw	3441	87	85	ν_{sym} NH_2 [100]
-	-	3432	110	685	ν_{sym} NH_2 [100]
3345m	-	3363	139	674	ν_{asym} NH_3^+ [99]
3321m	-	3358	104	97	ν_{asym} NH_3^+ [97]
3271m	-	3294	193	397	ν_{sym} NH_3^+ [8]
3216m	-	3239	139	242	ν_{asym} NH_3^+ [96]
3174m	3191w	3190	243	130	ν_{sym} NH_3^+ [95]
3068m	-	3025	25	480	ν_{asym} CH_2 [60] + ν C—H [29]
3009m	-	3000	14	757	ν_{asym} CH_2 [58] + ν C—H [27]
2985m	2993w	2991	24	743	ν_{asym} CH_2 [41] + ν C—H [20]
-	-	2964	19	386	ν_{sym} CH_2 [52] + ν C—H [17]
-	-	2948	34	753	ν_{sym} CH_2 [48] + ν C—H [15]
2931m	2945vs	2930	6	1809	ν_{sym} CH_2 [58]
2867m	2822vw	-	-	-	ν_{sym} CH_2 + ν_{sym} NH_3^+
2773w	2816vw	-	-	-	ν_{sym} NH_3^+
2715w	2712vw	-	-	-	ν_{sym} NH_3^+
2646w	-	2653	2090	325	ν N—H (NH_3^+) (bonded) [93]
2609w	-	-			ν_{sym} NH_3^+
2543w	-	-		-	ν_{sym} NH_3^+
2488w	-	-	-	-	ν_{sym} NH_3^+
2265vw	-	-	-	-	ν_{sym} NH_3^+
2045vw	-	-	-	-	Combination band (1585 cm^{-1} + 582 cm^{-1})
1685s	1690vw	-	-	-	ν C=O
1635vs	1632m	1615	61	190	δ_{sci} NH_3^+ [82]
1628vs	1611m	1606	441	45	δ_{sci} NH_3^+ [38] + δ_{sci} NH_2 [41] + ν CN [10]
1585s	-	1554			δ_{sci} NH_3^+ [40] + ν C=O [35]
-	1547w	1538	372	141	ν_{asym} COO^- [21] +δ_{wag} NH_3^+ [65]
1486s	1495w	1484	16	256	ν_{asym} COO^- [18] + δ_{wag} NH_3^+ [40]
-	-	1450	82	162	ν_{asym} COO^- [35] + δ_{wag} NH_3^+ [33] + ν C=O [11] + δ_{sci} CH_2 [12] + δ_{sci} CNH [8]
1449m	1447m	1441	1129	758	ν_{asym} COO^- [30] + δ_{wag} NH_3^+ [38] + ν C=O [8] + δ_{sci} CH_2 [15] + δ_{sci} CNH [10]
1412s	1416s	1415			δ_{sci} CH_2 [75] +δ_{wag} NH_3^+ [11]
-	-	1389	123	503	δ_{wag} CH_2 [59] + ν CC [24] + δ_{sci} HNC [15]
1359m	1356w	1363	181	471	δ_{wag} CH_2 [39] + ν CC [20] + δ_{sci} HNC [15] + δ_{sci} NCC [15]
1335s	1323s	1346	187	336	δ_{wag} NH_3^+ [9] +δ CH [34] + δ_{wag} CH_2 [32] + ν CN [10] + δ_{wag} CH_2 [17]
1315m	-	1311	100	511	δ_{twi} NH_3^+ [16] +δ COO^- [12] + ν CC [20] + δ_{sci} NH_2 [8]
1281m	1297w	1294	45	603	δ_{sci} COO^- [18] + δ CH [9] + δ_{wag} CH_2 [29] ν CC [25]
-	-	1277	98	461	δ_{twi} CH_2 [25] +δ CH [35] + δ_{sci} COO^- [10] + ν CC [15]
1250w	1254w	1259	20	801	δ_{twi} CH_2 [55] + δ_{roc} NH_3^+ [16] + δ_{sci} COO^- [8] +δ CH [18]
1200w	1204w	1242	125	299	δ_{twi} NH_3^+ + δ_{wag} CH_2 [65] +δ_{sci} COO^- [30] + δ_{roc} NH_3^+ [18] + δ CH [14]
-	-	1207	76	273	δ_{twi} NH_3^+ [35] + δ_{twi} CH_2 [10] + ν CC [10]
-	-	1190	90	510	δ_{twi} NH_3^+ + δ_{twi} CH_2 [20] + δ_{wag} CH_2 [18] + δ_{roc} NH_2 [5] + ν CC [10] + δ_{sci} COO^- [8]
1163m	1162m	1164	86	232	δ_{twi} NH_3^+ [20] + δ_{twi} CH_2 [25] + δ CH [10] + ν CC [12] + δ_{sci} COO^- [10] + δ_{roc} NH_2 [10]

Continued of Table 12.

wavenumber in cm^{-1}			D-I Intensity		Assignment
IR	Raman	D-I	IR	Raman	
1126w	1133w	1110	137	430	δ_{twi} NH_3^+ [25] + δ_{twi} CH_2 [15] + δ CH [30] + δ HCC [10]
1086w	1096m	1086	106	135	δ_{twi} NH_3^+ [28] + δ_{twi} CH_2 [18] + δ CH [15] + δ_{roc} NH_2 [10]
1048w	1048w	1060	63	124	δ_{roc} NH_2 [25] + ν CC [12] + ν CN [12] + ν C=O [10] + δ_{roc} CH_2 [12] + δ CCN [11]
-	1000w	1008	40	516	δ_{roc} NH_2 [15] + ν CC [15] + ν CN [10] + ν C=O [10] + δ_{twi} CH_2 [12] + δ OCC [12]
995w	-	990	32	671	δ_{twi} NH_3^+ [28] + δ_{roc} NH_2 [15] + ν CC [25] + δ_{twi} CH_2 [22]
985vw	-	956	26	428	δ_{twi} NH_3^+ [22] + ν CN [12] + δ_{roc} NH_2 [10] + δ_{roc} CH_2 [15]
935vw	928w	912	16	624	δ_{roc} CH_2 [11] + ν CN [22] + δ OCC [10] + δ_{roc} NH_2 [8]
895vw	896m	896	3	238	δ_{roc} NH_3^+ [15] + δ CCC [12] + δ_{roc} CH_2 [28] + ν CN [20]
878vw	-	861	28	224	δ_{roc} CH_2 [15] +δ CCC [10] + δ_{sci} COO^- [12] + δ_{roc} NH_3^+ [10]
844w	850s	835	25	805	τ HNHO [20] + ν CC [25] + ν CN [15] + δ CCC [20]
806w	809w	818	10	264	δ_{roc} CH_2 [12] +δ_{roc} NH_3^+ [10] + δ_{sci} COO^- [14] + ν CC [20] + ν CN [12] + δ CCC [15]
773w	778w	774	4	797	δ_{roc} NH_2 [20] + τ CCCC [25] + τ HCCH [25]
754vw	-	731	76	131	δ_{roc} CH_2 [25] + δ_{roc} NH_2 [15] + δ_{sci} COO^- [18]
721vw	-	713	66	96	δ_{roc} CH_2 [15] + δ_{sci} COO^- [10] + δ CCC [15] + τ HNCO [25] + τ CCCC [12]
679w	-	671	28	860	δ_{roc} CH_2 [15] + δ COO^- [10] + δ_{roc} NH_3^+ + τ CCCC
654w	649w	-	-	-	δ_{roc} CH_2 [15] + τ HNCC [18] + τ CCCC [12]
622w	620w	619	82	1018	$\delta_{twi}NH_2$ [20] + τ HNCO [12] + τ CCCN [10] + τ CCCC [15]
582w	-	593	109	598	$\delta_{twi}NH_2$ [22] + δ COO^- [12] + τ CCCN [10] + τ CCCC [15]
534s	548w	-	-	-	δ NH_2 [28] + τ HNCC [25]
477w	479w	506	238	131	δ NCC + τ HNHC + ONH$\cdots$OC [25] + τ NCOH [15]
457w	446w	454	36	973	τ HNHC [10] + OUT NCOH [15] + τ CCCC [15]
-	421w	402	24	207	δ NCC [15] + δ_{roc} CH_2 [22] + δ_{roc} NH_2 [20] + τ CCCC [12] + τ CCCC [15]
-	338w	376	23	442	δ_{roc} CH_2 [20] + τ CCCC [12] + τ HCCH [15] + δ_{roc} NH_3^+ [25]
-	-	359	0.45	467	δ_{roc} NH_3^+ [35] + δ_{roc} CH_2 [15] + OUT OCCH [10]
-	-	333	55	437	δ_{roc} NH_3^+ [15] + δ_{roc} CH_2 [10] + OUT OCCN [20]
-	286w	309	73	1121	δ_{roc} NH_3^+ [25] + δ_{roc} CH_2 [15] + τ OCCN [20] +τ CCCC [12] + τ HCCH [15]
-	-	246	41	218	δ_{roc} NH_3^+ [25] + δ_{roc} CH_2 [15] + τ NH$\cdots$OC [25] + τ OCCN [20] + τ CCCC [15] + τ HCCO [12]
-	209w	212	23	438	δ_{roc} NH_3^+ [10] + δ_{roc} CH_2 [12] + τ NH$\cdots$OC [30] + τ OCCN [15] + τ CCCC [28] + τ HCCO [12]
-	182w	186	10	509	δ_{roc} CH_2 [22] + τ NH$\cdots$OC [18] + τ HNCH [10] + τ CCCC [12] + τ OCNH [12]
-	-	168	45	392	δ_{roc} NH_3^+ [10] + δ_{roc} CH_2 [12] + τ NH$\cdots$OC [30] + τ OCCN [15] + τ CCCC [28] + τ HCCO [12]
-	131w	134	19	392	τ NH$\cdots$OC [25] + τ OCCN [18] + τ CCCC [30] + τ HCCO [32]
-	109s	108	37	1935	δ_{roc} CH_2 [20] + δ_{roc} NH_2 [22] + τ NH$\cdots$OC [28] + τ HNCC [25] + τ CCCC [30] + τ HCCO [15]
-	80w	82	60	2004	δ_{roc} CH_2 [20] + δ_{roc} NH_2 [22] + τ NH$\cdots$OC [28] + τ HNCC [25] + τ OCCN [15] + τ HCCC [28] + τ HCCO [12]
-	-	64	11	8119	τ NH$\cdots$OC [15] + τ CCCC [20] + τ HCCO [22] τ OCCN [18] + τ HCCC [18]
-	-	38	31	1046	τ NH$\cdots$OC [20] + τ OCCN [11] + τ CCCC [28] + τ HCCO [12] + τ HCCC [25]
-	-	12	22	2647	τ NH$\cdots$OC [30] + τ OCCN [15] + τ CCCC [28] + τ HCCO [12] + τ HCCC [32]

Note: ν- stretching, δ- bending, τ- torsional, OUT- out of plane bending, computed vibrational frequencies are scaled by scaling factor of 0.968 [26]. The percentage values of the potential energy distribution are given in square brackets.

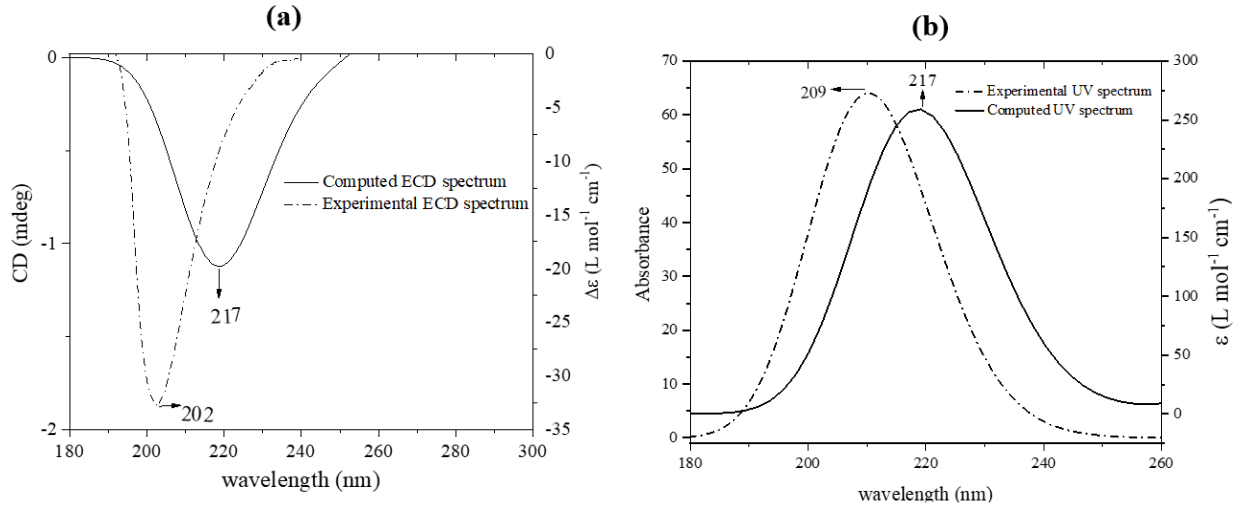

Figure 11. (a) ECD spectrum and (b) UV-Vis spectrum of D-Glutamine at a concentration of 5 mM (dashed line) with computed spectra of D-I at the TD-DFT CAM-B3LYP/6-31G level (solid line).

more stabilization energy than *intra*- N—H···O bonding. The N—H···O corresponds to the charge transfer from the O lone pair orbital (donor) to the N—H antibonding orbital (acceptor). Here, n_2 (COO^-) $\rightarrow$ σ*(N—H) showed maximum stabilization energy $E^{(2)}$ = 33.5 kcal/mol, indicating greater orbital overlapping. With both *inter*- and *intra*- N—H···O bond orbital overlapping pictures in D-I are shown in figure 12 [35–37].

3.6.2 Molecular electrostatic potential analysis

MEP is a useful technique to understand H-bonding and the reactivity of molecules. It indicates a visual method for understanding positive, negative, and neutral electrostatic potential regions using color coding method [12, 38]. The MEP surface of the D-I species was calculated from the optimized molecular structure of D-I and is shown in figure 13. The different values of electrostatic potentials at the MEP surface are represented by different colors: red, blue, and green represent the regions of most negative, most positive, and zero electrostatic potential, respectively. The negative region is localized over COO^- group, indicating the most reactive site for electrophilic attack, and the positive region is localized over the NH_3^+ group, which is a reactive site for nucleophilic attack. The loss of red and blue colors on COO^- and NH_3^+ groups in the bonding region of the D-I species indicates N—H···O bonding interaction.

3.6.3 HOMO-LUMO analysis

Since *intra*-/*inter*- H-bonding is all about charge transfer between frontier orbitals represented by the HOMO-LUMO, yielding energy gaps between HOMO and LUMO [34, 39–44]. The frontier molecular orbital energies were obtained for M_{ZW} and D-I species of D-Gln. The LUMO as an electron acceptor represents the ability to accept an electron, while HOMO represents the ability to donate the electron. The 3D plots of the frontier orbitals; the HOMO and LUMO, are shown in figure 14 for M_{ZW} and D-I. The HOMO-LUMO energy gap describes the chemical stability and the eventual charge transfer in a molecule. The large HOMO-LUMO energy gap of 7.76 eV for the M_{ZW} indicates that it is more stable and unreactive. There is a decrease in HOMO-LUMO energy gap from M_{ZW} 7.76 eV

Table 13. Stabilization energy values of N—H···O bonded D-I dimer of D-Glutamine at DFT B3LYP/6-31G(d,p) level.

N—H···O Bond	Donor NBO (i)	Acceptor NBO (j)	$E^{(2)}$ kcal/mol
inter-molecular	n_1 O15	σ*(N 27 - H 33)	08.1
	n_2 O15	σ*(N 27 - H 33)	33.5
	n_3 O15	σ*(N 27 - H 33)	00.7
intra-molecular	n_1 O17	σ*(N 7 - H 16)	00.8
	n_2 O17	σ*(N 7 - H 16)	02.4
	n_1 O34	σ*(N 7 - H 14)	04.5
	n_2 O34	σ*(N 7 - H 14)	16.8
	n_1 O34	σ*(N 27 - H 32)	01.8
	n_2 O34	σ*(N 27- H 32)	07.5
	n_2 O35	σ*(C23-H30)	01.0

Note: n - lone pair orbital, σ* - antibonding orbital, $E^{(2)}$ - Stabilization energy.

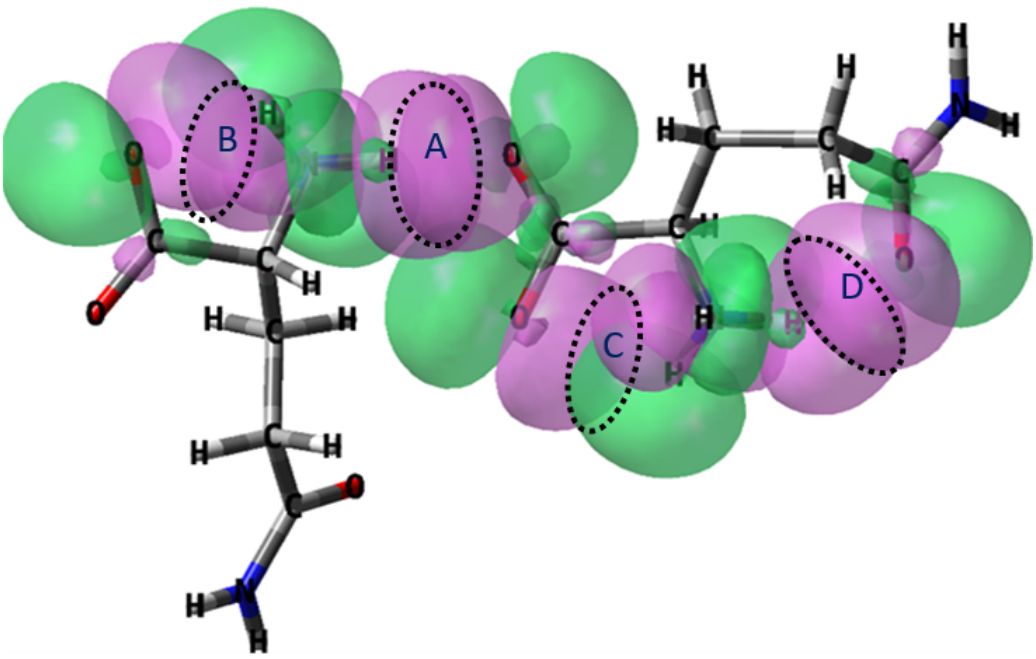

Figure 12. Overlapping of the hybrid orbitals highlighting N—H···O bonding in dimer D-I of D-Glutamine. Dotted line represents orbital overlapping region due to *inter*-(A) and *intra*- (B, C, D) N—H···O bonding.

to D-I 7.59 eV. This decrease in energy is due to N—H···O bonding in D-I [11].

3.6.4 AIM and NCI analysis

The *inter*-/*intra*- molecular interactions for D-I have been further studied through AIM and NCI analysis. AIM can be used to characterize H-bonding between donor and acceptor groups, which is characterized by the presence of bond critical points (BCP) corresponding to (3, −1) and is shown in figure 15 [45–48]. BCP points 50 (N—H···O), 61 (C—H···O), 74 (C—H···O), and 88 (N—H···O), 83(N—H···O), 41 (N—H···O), 60 (C—H···O) indicate *inter*- and *intra*- bonding in D-I respectively. Topological parameters such as total molecular electronic density $\rho(r)$, Laplacian electronic density $\nabla^2\rho(r)$, and E_{HB}. According to the interactions of H-bonds can be defined as follows:

1. $\nabla^2\rho(r) > 0$ and $H(r) > 0$: Weak H-bonds
2. $\nabla^2\rho(r) > 0$ and $H(r) < 0$: Strong H-bonds
3. $\nabla^2\rho(r) < 0$ and $H(r) < 0$: Very strong H-bonds

The calculations for a characterization of the H-bond were done at the B3LYP/6-31G(d,p) level. We observed D-I *inter*-

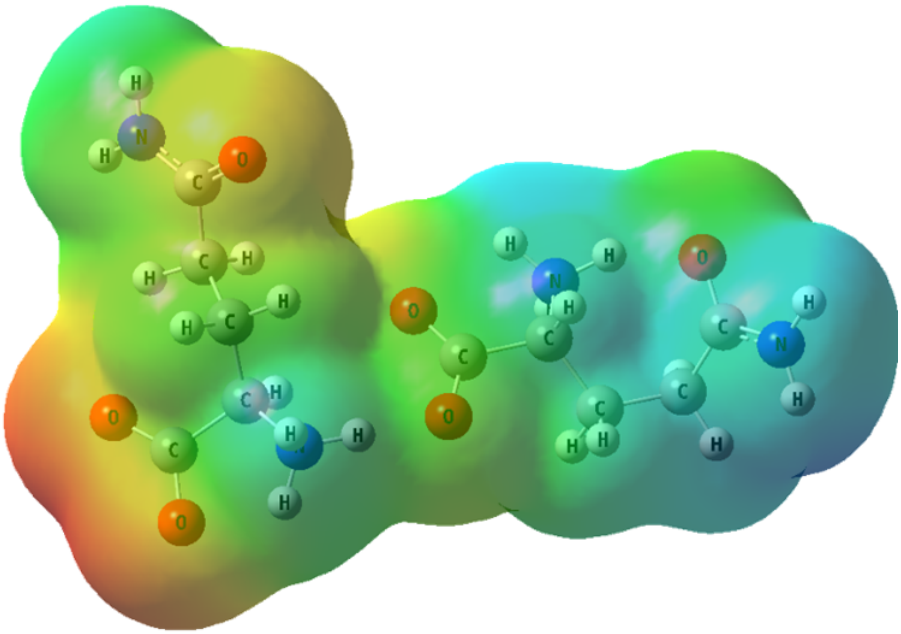

Figure 13. Molecular electrostatic potential surface for N—H···O bonded D-I of D-Gln.

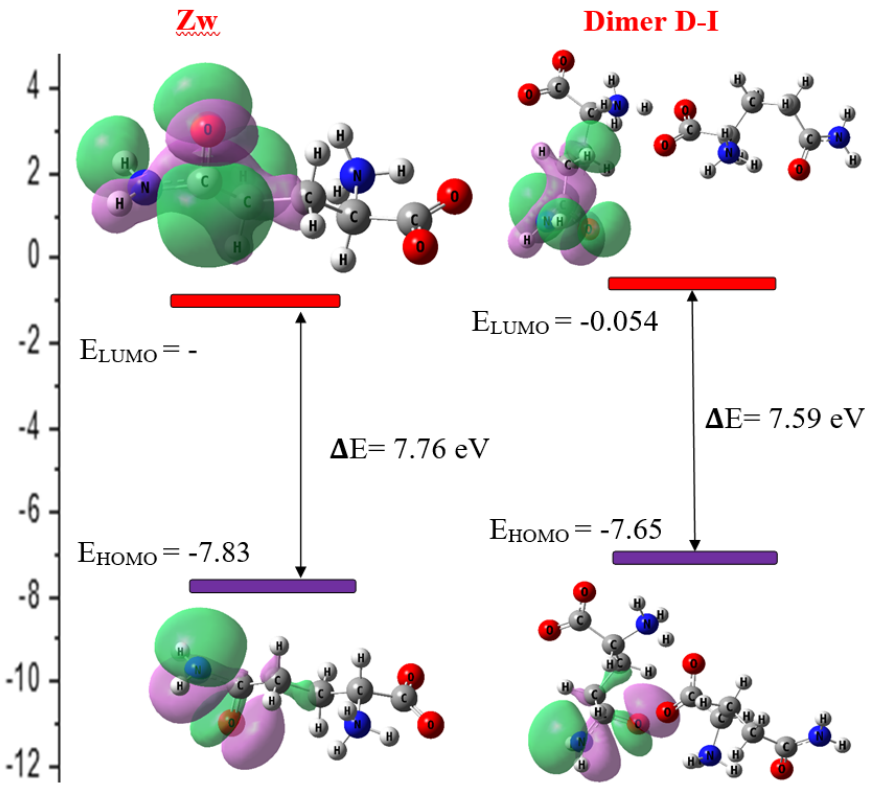

Figure 14. Molecular orbital surfaces for HOMO and LUMO for zwitterionic monomer M_{ZW} and dimer D-I of D-Glutamine arranged in order of their energies.

N—H···O bond with $\nabla^2\rho(r)$ is equal to 0.167 a.u. which is greater than zero and $H(r)$ is equal to -0.00263 a.u. which is less than zero; therefore, it indicates strong H-bonds. Equation (1) has been used to calculate the N—H···O bond interaction energy at BCP.

$$E_{HB} = \frac{V(r)}{2} \text{ kcal/mol} \tag{1}$$

NCI in the molecular systems can be visualized using reduced density gradient (RDG). The RDG is given by:

$$S = \frac{|\nabla\rho(r)|}{2(3\pi^2)^{1/3}|\rho(r)^{4/3}|} \tag{2}$$

where $\rho(r)$ is the electron density and $\nabla\rho(r)$ is its gradient. By using colour codes, NCI isosurfaces show how interactions behave in actual space [49–53]. NCI isosurfaces and

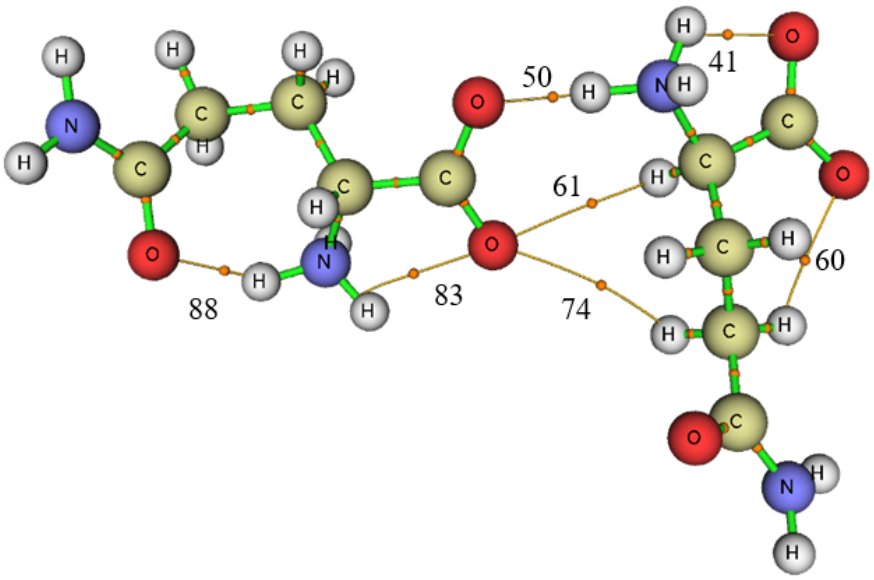

Figure 15. Molecular structure of N—H···O bonded dimer D-I of D-Glutamine, with bond critical points (orange dots) corresponding to (3, -1). The BCP points were marked with numbers.

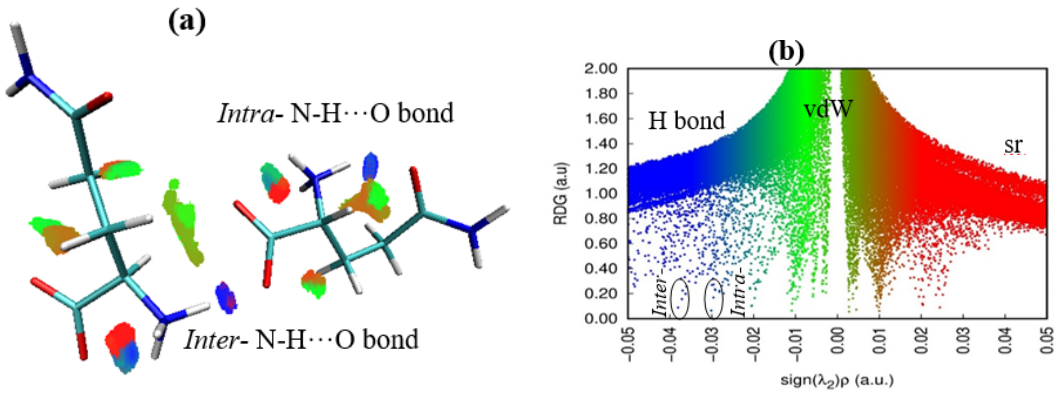

Figure 16. (a) 3-D isosurfaces and (b) 2D scatter plots of the sign(λ_2) $\rho(r)$ versus RDG and corresponding isosurfaces of dimer D-I of D-Glutamine. The colour gradient corresponds to the three interaction types shown on it. (H bond: hydrogen bond, vdW: van der Waal, sr: steric repulsion).

corresponding 2-D scatter plots for D-I are shown in figure 16a and figure 16b, respectively. Red colour isosurfaces indicate a repulsive interaction, while green-red colour isosurfaces indicate a weak van der Waals interaction, and blue denotes H-bonding. Blue isosurfaces between the NH_3^+ and COO^- group indicate the N—H···O bonding D-I. 2D scattered graphs for D-I structure, showing steric repulsion (sr) interaction when $\lambda_2 > 0$ and the van der Waals (vdW) and H-bond interactions (H bond) when $\lambda_2 < 0$. Low-gradient with high-density spike at sign $(\lambda_2)\rho(r) = -0.03$ a.u indicated to the *intra-* molecular N—H···O bonding; similarly, sign $(\lambda_2)\rho(r) = -0.04$ a.u indicates the *inter-* molecular N—H···O bonding, suggesting the *inter-* molecular N—H···O bonding is stronger than the *intra-* molecular N—H···O bonding.

4. Conclusion

In the present study, we have reported N—H···O bonded dimer species for D-Glutamine from MD simulations and DFT analysis. We scanned the neutral monomer structure of D-Glutamine for different dihedral angles, which are responsible for the non-rigidity of the molecule, and obtained the minimum energy structure. The XRD and monomer paper reported that Glutamine exists in the zwitterion phase. In *Gaussian 09W*, Glutamine exists neutral in the gas phase. So, we optimized monomer structure at B3LYP/6-311++G (d,p) with implicit solvation using the SMD model water as solvent. It yielded a zwitterion monomer structure. This optimized structure was further used as an input structure for MD simulation. We performed MD simulations for 1 ns, equilibration runs at 300 K temperature and 1 bar pressure. During simulation, we observed *intra-* and *inter-* molecular N—H···O bonded non-closed dimer, closed dimer, trimer, and tetramer species. We calculated the maximum residence time for all oligomers. For D-Glutamine, four types of *inter-* molecular N—H···O bonding. From each dimer group, the dimer with the greater maximum residence time value, 180, 170, 160 and 100 ps renamed as D-I, D-II, D-III and D-IV, respectively. They were considered for optimization, vibrational frequency, NBO and AIM analysis at B3LYP/6-31G(d,p) level. Dimer D-I has a 180 ps maximum residence time value, which is greater among all; In RDF analysis, r_{max} at 1.68 Å which is less than 2.72 Å (the sum of van der Waals radii of O and H), and the minimum among others and this indicates the presence of strong N—H···O bonding in D-I; For D-I, the N—H···O bond angle is 179.9°, indicates linear bonds are stronger than non-linear bonds; there is 21% frequency shift between bonded and non-bonded N—H stretching which indicates stronger the N—H···O bond in D-I; Stabilization energy from NBO theory is 33.5 kcal/mol which is greater than all others, indicating stronger the N—H···O bond in D-I; we calculated H-bond interaction energy from AIM analysis which is −14.7 kcal/mol which indicates stronger N—H···O bond in D-I. In all previous results, Dimer D-I shows a strong N—H···O bond. So, we consider the D-I dimer structure for further detailed analysis. We compared optimized parameters with the neutron diffraction data and calculated mean absolute deviations and root mean square error for D-I. D-I is in very good agreement with the reported XRD structure; Vibrational bands D-I are in good agreement with experimental IR and Raman bands. We computed the ECD and UV-Vis spectrum for D-I using the TD-DFT method, and compared it with the corresponding experimental spectra. We observed 7% and 4% deviation for ECD and UV-Vis spectra, respectively. This N—H···O bond was further electronically characterized by NBO, MEP, HOMO & LUMO, AIM, and NCI analysis. From NBO analysis D-I with stabilization energy $E^{(2)}$ = 33.5 kcal/mol and greater orbital overlapping between $n(COO^-) \rightarrow \sigma^*$(N—H) indicates stronger N—H···O bonding in D-I. From the MEP surface, the loss of red and blue colors on -COO^- and - NH_3^+ groups respectively, in the bonding region of the D-I species indicates N—H···O bonding in D-I. There is a decrease in HOMO-LUMO energy gap from monomer 7.76 eV to D-I dimer energy gap 7.59 eV, which indicates strong N—H···O bonding in D-I. From AIM analysis, D-I with H-bond interaction energy $E_{HB} = -14.7$ kcal/mol at BCP point corresponding to (3, −1) indicates stronger N—H···O bonding in D-I. From NCI analysis Low-gradient with high-density spike at sign $(\lambda_2)\rho(r) = -0.030$ a.u is attributed to the *intra-* molecular N7-H16···O17 bonding in D-I species; similarly, sign $(\lambda_2)\rho(r) = -0.039$ a.u indicates the *inter-* molecular

N27-H33···O15 bonding. Suggesting the *inter*- molecular interaction is stronger than the *intra*- molecular interaction. Therefore, the computed D-I spectrum is in good agreement with the experimental IR, Raman, UV-Vis, and ECD spectra. All the analyses are consistent and good agree well with the experimental results.

Acknowledgment
The authors are thankful to USIC and SAIF, Karnatak University, Dharwad, for instrumentation facilities. Mithil Kotyagol sincerely appreciates the financial support received through the National Fellowship for ST Students sponsored by the Ministry of Tribal Affairs, Government of India. Additionally, we thank Prof. S. Umapathy for a visit by Prof. Jayashree Tonannavar to his MD computational lab at the Department of IPC, Indian Institute of Science, Bengaluru.

Authors Contribution
The intellectual substance, idea, and design of this study, or the analysis and interpretation of the data (if applicable), as well as the manuscript's writing, were all sufficiently contributed to by each author.

Availability of data and materials
The data that support the findings of this study are available from the corresponding author upon reasonable request.

Conflict of interests
The authors declare that they have no known competing financial interests or personal relationships that could have appeared to influence the work reported in this paper.

References

[1] Q. Du, X. Zhang, X. Pan, H. Zhang, Y.S. Yang, J. Liu, and Q. Jiao. "A novel strategy for efficient chemoenzymatic synthesis of D-Glutamine using recombinant Escherichia coli cells.". *J Mol Struct*, **1219**, 2020.
DOI: https://doi.org/10.1016/j.molstruc.2020.128600.

[2] M. Z. Abidin, T. Saravanan, E. Strauss, and G. J. Poelarends. "The broad amine scope of pantothenate synthetase enables the synthesis of pharmaceutically relevant amides.". *Org Biomol Chem*, **19**:4515–4519, 2021.
DOI: https://doi.org/10.1039/d1ob00238d.

[3] W. Cochran and B. R. Penfold. "The Crystal Structure of L-Glutamine.". *Acta Cryst*, **5**:644–653, 1952.
DOI: https://doi.org/10.1107/S0365110X52001775.

[4] T. F. Koetzle, M. N. Frey, M. S. Lehmann, and C. H. William. "Precision neutron diffraction structure determination of protein and nucleic acid components. XIII. Molecular and crystal structure of the amino acid L-glutamine.". *Acta Crystallographica Section B*, 1973.
DOI: https://doi.org/10.1107/S0567740873007028.

[5] A. Pawlukojc, K. Hołderna-Natkaniec, G. Bator, and I. Natkaniec. "L-Glutamine: Dynamical properties investigation by means of INS, IR, Raman, ^{1}H NMR and DFT techniques.". *Chem Phys*, **443**:17–25, 2014.
DOI: https://doi.org/10.1016/j.chemphys.2014.08.003.

[6] N. H. Rhys, A. K. Soper, and L. Dougan. "The hydrogen-bonding ability of the amino acid Glutamine revealed by neutron diffraction experiments.". *Journal of Physical Chemistry B*, **116**:13308–13319, 2012.
DOI: https://doi.org/10.1021/jp307442f.

[7] R. Ding, J. Ying, and Y. Zhao. "An electronic circular dichroism spectroscopy method for the quantification of L- and D-amino acids in enantiomeric mixtures.". *R Soc Open Sci*, **8**, 2021.
DOI: https://doi.org/10.1098/rsos.201963.

[8] M. J. Frisch, G. W. Trucks, H. B. Schlegel, G. E. Scuseria, M. A. Robb, J. R. Cheeseman, G. Scalmani, V. Barone, B. Mennucci, G. A. Petersson, H. Nakatsuji, M. Caricato, X. Li, H. P. Hratchian, A. F. Izmaylov, J. Bloino, G. Zheng, J.L. Sonnenberg, M. Hada, M. Ehara, K. Toyota, R. Fukuda, J. Hasegawa, T. Ishida, T. Nakajima, Y. Honda, O. Kitao, H. Nakai, T. Vreven, J. A. Montgomery Jr., J. E. Peralta, F. Ogliaro, M. Bearpark, J.J. Heyd, E. Brothers, K. N. Kudin, V. N. Staroverov, R. Kobayashi, J. Normand, K. Raghavachari, A. Rendell, J. C. Burant, S. S. Iyengar, M. Tomasi, N. Cossi, N. Rega, Millam, et al. "Gaussian 09, Revision D.01.". 2009.

[9] R. Dennington, T. Keith, and J. Millam. "GaussView 5.0.". 2009.

[10] M. H. Jamroz. "Vibrational energy distribution analysis (VEDA): scopes and limitations.". *Spectrochim. Acta – Part A Mol. Biomol. Spectrosc.*, **114**:220–230, 2013.
DOI: https://doi.org/10.1016/j.saa.2013.05.096.

[11] M. D. Prabhu, Jayashree Tonannavar, and J. Tonannavar. "Multiple-H-bonded-zwitterionic tetramer structure for L-(+)-2-chlorophenylglycine, as investigated by UV, IR and Raman spectroscopy and electronic structure calculations.". *J Mol Struct*, **1246**, 2021.
DOI: https://doi.org/10.1016/j.molstruc.2021.131218.

[12] S. Yalagi, J. Tonannavar, and Jayashree Tonannavar. "DL-3-Aminoisobutyric acid: vibrational, NBO and AIM analysis of N–H···O bonded-zwitterionic dimer model.". *Heliyon*, **5**, 2019.
DOI: https://doi.org/10.1016/j.heliyon.2019.e01933.

[13] A. V. Marenich, C. J. Cramer, and D. G. Truhlar. "Universal Solvation Model Based on Solute Electron Density and on a Continuum Model of the Solvent Defined by the Bulk Dielectric Constant and Atomic Surface Tensions.". *The Journal of Physical Chemistry B*, **113**, 2009.
DOI: https://doi.org/10.1021/jp810292n.

[14] M. J. Abraham, D. van der Spoel, E. Lindahl, B. Hess, and the GROMACS development team. "GROMACS User Manual version.". 2019.

[15] H. J. C. Berendsen, D. van der Spoel, and R. van Drunen. "GROMACS: A message-passing parallel molecular dynamics implementation.". *Comput Phys Commun*, **91**, 1995.
DOI: https://doi.org/10.1016/0010-4655(95)00042-E.

[16] D. Van Der Spoel, E. Lindahl, B. Hess, G. Groenhof, A. E. Mark, and H. J. C. Berendsen. "GROMACS: Fast, flexible, and free.". *J Comput Chem*, **26**:1701–1718, 2005.
DOI: https://doi.org/10.1002/jcc.20291.

[17] P. Szilard, M. J. Abraham, C. Kutzner, B. Hess, and E. Lindahl. "Tackling Exascale Software Challenges in Molecular Dynamics Simulations with GROMACS.". *Computer Science*, 2015.

[18] L. Pallavi, J. Tonannavar, and Jayashree Tonannavar. "Molecular dynamics simulation, DFT calculations and vibrational spectroscopic study of N-H···O bound dimer models for DL-β-phenylalanine and 3-amino-3-(4-chlorophenyl)propionic acid.". *J Mol Liq*, **352**, 2022.
DOI: https://doi.org/10.1016/j.molliq.2022.118746.

[19] R. P. Kavali, Jayashree Tonannavar, J. Bhovi, and J. Tonannavar. "Study of O–H···O bonded-cyclic dimer for 2,5-Dihydroxyterephthalic acid as aided by MD, DFT calculations and IR, Raman, NMR spectroscopy.". *J Mol Struct*, **1264**, 2022.
DOI: https://doi.org/10.1016/j.molstruc.2022.133174.

[20] B. Hess, H. Bekker, H.J.C. Berendsen, and J. G. E. M. Fraaije. "LINCS: A Linear Constraint Solver for Molecular Simulations.". *J Comp Chem*, 1997.
DOI: https://doi.org/10.1002/(SICI)1096-987X(199709).

[21] U. Essmann, L. Perera, M. L. Berkowitz, T. Darden, H. Lee, and L. G. Pedersen. "A smooth particle mesh Ewald method.". *J Chem Phys*, **103**:8577–8593, 1995.
DOI: https://doi.org/10.1063/1.470117.

[22] P. N. Patrone and T. W. Rosch. "Beyond histograms: efficiently estimating radial distribution functions via spectral Monte Carlo.". *J Chem Phys*, 2017.
DOI: https://doi.org/10.1063/1.4977516.

[23] C. J. Cramer. "Essential of computational chemistry book Theories and models.". 2004.

[24] A. Subhasri, S. Balachandran, K. Mohanraj, P. S. Kumar, K. J. Jothi, and C. Anbuselvan. "Synthesis, Computational and Cytotoxicity Studies of Aryl Hydrazones of β-Diketones: Selective Ni^{2+} Metal Responsive Fluorescent Chemosensors.". *Chemosphere*, **297**:134150, 2022.
DOI: https://doi.org/10.1016/j.chemosphere.2022.134150.

[25] T. Hodson. "Root-mean-square error (RMSE) or mean absolute error (MAE): when to use them or not, Geoscientific Model Development.". 2022.
DOI: https://doi.org/10.5194/gmd-15-5481-2022.

[26] E. Rudberg, E. H. Rubensson, and P. Sałek. "Hartree-Fock calculations with linearly scaling memory usage.". *J Chem Phy*, **128**, 2008.
DOI: https://doi.org/10.1063/1.2918357.

[27] G. R. Desiraju. "Weak hydrogen bonds in crystal engineering.". *Chem Comm*, 2005.
DOI: https://doi.org/10.1039/B504372G.

[28] N. B. Colthup, L. H. Daly, S. E. Wiberley, and W. Liptay. "Introduction to Infrared and Raman Spectroscopy.". *Chemie International Edition in English*, **4**, 1965.
DOI: https://doi.org/10.1002/anie.196507241.

[29] H. W. Thompson and L. J. Bellamy. "The infra-red spectra of complex molecules.". *Spectrochimica Acta*, **7**, 1955.
DOI: https://doi.org/10.1016/0371-1951(55)80034-3.

[30] G. Socrates. "Infrared and Raman characteristic group frequencies.". 2001.

[31] D. A. Skoog, F. J. Holler, and S. R. Crouch. "Principles of Instrumental Analysis.". 2016.

[32] A. E. Reed, L. A. Curtiss, and F. Weinhold. "Intermolecular Interactions from a Natural Bond Orbital, Donor—Acceptor Viewpoint.". *Chem Rev*, **88**, 1988.
DOI: https://doi.org/10.1021/cr00088a005.

[33] E. D. Glendening, C. R. Landis, and F. Weinhold. "Natural bond orbital methods.". *Wiley Interdiscip Rev Comput Mol Sci*, **2**:1–42, 2012.
DOI: https://doi.org/10.1002/wcms.51.

[34] V. Krishnakumar, D. Barathi, R. Mathammal, J. Balamani, and N. Jayamani. "Spectroscopic properties, NLO, HOMO-LUMO and NBO of maltol.". *Spectrochim Acta A Mol Biomol Spectrosc*, **121**: 245–253, 2014.
DOI: https://doi.org/10.1016/j.saa.2013.10.068.

[35] P. Ramanna, Jayashree Tonannavar, and J. Tonannavar. "Study of H-bonded cyclic dimer of organic linker 5-Bromoisophthalic acid by DFT and vibrational spectroscopy.". *J Mol Struct*, **1241**, 2021.
DOI: https://doi.org/10.1016/j.molstruc.2021.130613.

[36] S. Yalagi, J. Tonannavar, and J. Yenagi. "Experimental and DFT dimer modeling studies of the H-bond induced-vibration modes of L-β-Homoserine.". *Spectrochim Acta A Mol Biomol Spectrosc*, **181**: 109–115, 2017.
DOI: https://doi.org/10.1016/j.saa.2017.03.041.

[37] E. Kvasyuk, A. Sysa, S. Al Saud, S. Shahab, M. Sheikhi, S. Kaviani, and A. Zinchenko. "Quantum Chemical Modeling, Synthesis, Spectroscopic (FT-IR, Excited States, UV/Vis) Studies, FMO, QTAIM, ELF, LOL, NBO, NLO and QSAR Analyses of Nelarabine.". *Biointerface Research in Applied Chemistry*, **13**(2):144, 2023.
DOI: https://doi.org/10.33263/BRIAC132.144.

[38] C. M. Breneman and K. B. Wiberg. "Determining atom-centered monopoles from molecular electrostatic potentials. The need for high sampling density in formamide conformational analysis.". *J Comp Chem*, **11**, 1990.
DOI: https://doi.org/10.1002/jcc.540110311.

[39] M. Saranya, S. Ayyappan, R. Nithya, R. K. Sangeetha, and A. Gokila. "Molecular Structure, NBO And HOMO-LUMO Analysis of Quercetin on Single Layer Graphene by Density Functional Theory.". *Digest Journal of Nanomaterials and Biostructures*, **13**:97–105, 2018.

[40] N. Issaoui, H. Ghalla, S. Muthu, H.T. Flakus, and B. Oujia. "Molecular structure, vibrational spectra, AIM, HOMO-LUMO, NBO, UV, first order hyperpolarizability, analysis of 3-thiophenecarboxylic acid monomer and dimer by Hartree-Fock and density functional theory.". *Spectrochim Acta A Mol Biomol Spectrosc*, **136**:1227–1242, 2015.
DOI: https://doi.org/10.1016/j.saa.2014.10.008.

[41] N. Choudhary, S. Bee, A. Gupta, and P. Tandon. "Comparative vibrational spectroscopic studies, HOMO-LUMO and NBO analysis of N-(phenyl)-2,2-dichloroacetamide, N-(2-chloro phenyl)-2,2-dichloroacetamide and N-(4-chloro phenyl)-2,2-dichloroacetamide based on density functional theory.". *Comput Theor Chem*, **1016**: 8–21, 2013.
DOI: https://doi.org/10.1016/j.comptc.2013.04.008.

[42] M. D. Prabhu, Jayashree Tonannavar, V. Kamat, and J. Tonannavar. "XRD structure and vibrational analysis of DL-β-Leucine, as aided by DFT tetramer model and characterized by NBO, AIM and NCI calculations.". *J Mol Struct*, **1218**, 2020.
DOI: https://doi.org/10.1016/j.molstruc.2020.128495.

[43] H. A. Almodarresiyeh, S. Shahab, S. Kaviani, Z. I. Kuvaeva, H. G. Karankevich, M. M. Markovich, V. A. Kaminskaya, L. Filippovich, and M. Sheikhi. "Synthesis, DFT, Spectroscopic Studies and Electronic Properties of Novel Arginine Derivatives.". *Russian Journal of Physical Chemistry B*, **17**(1):12–26, 2023.
DOI: https://doi.org/10.1134/S1990793123010165.

[44] S. Shahab, M. Sheikhi, M. Khancheuski, H. Yahyaei, H. A. Almodarresiyeh, and S. Kaviani. "DFT, molecular docking and ADME prediction of tenofovir drug as a promising therapeutic inhibitor of SARS-CoV-2 Mpro.". *Main Group Chemistry*, **22**:115–128, 2023.
DOI: https://doi.org/10.3233/MGC-220046.

[45] R. F. W. Bader. "A Quantum Theory of Molecular Structure and Its Applications.". *Chemical Reviews*, 1991.

[46] S. S. Malaganvi, J. Tonannavar, and J. Tonannavar. "Experimental, DFT dimeric modeling and AIM study of H-bond-mediated composite vibrational structure of Chelidonic acid.". *Heliyon*, **5**, 2019.
DOI: https://doi.org/10.1016/j.heliyon.2019.e01586.

[47] S. S. Malaganvi, J. Tonannavar, and J. Tonannavar. "Spectroscopic and electronic structure characterization of H-bonding in 2-Bromohydroquinone.". *J Mol Struct*, **1181**:71–82, 2019.
DOI: https://doi.org/10.1016/j.molstruc.2018.12.063.

[48] P. L. A. Popelier. "Characterization of a Dihydrogen Bond on the Basis of the Electron Density.". 1998.

[49] E. R. Johnson, S. Keinan, P. Mori-Sánchez, J. Contreras-García, A. J. Cohen, and W. Yang. "Revealing noncovalent interactions.". *J Am Chem Soc*, **132**:6498–6506, 2010.
DOI: https://doi.org/10.1021/ja100936w.

[50] J. Bhovi, J. Tonannavar, and Jayashree Tonannavar. "IR, Raman spectroscopic, DFT, AIM and NCI characterization of O-H$\cdots$O/$\pi\cdots\pi$ bonds in dimer and trimer species as computed from MD simulations in water for Protocatechuic acid.". *J Mol Struct*, **1299**, 2024.
DOI: https://doi.org/10.1016/j.molstruc.2023.137077.

[51] L. Pallavi, J. Tonannavar, and Jayashree Tonannavar. "DFT zwitterion model for vibrational and electronic structure of unnatural 3-amino-3-(4-fluorophenyl)propionic acid, aided by IR and Raman spectroscopy.". *J Mol Struct*, **1211**, 2020.
DOI: https://doi.org/10.1016/j.molstruc.2020.128085.

[52] M. Kotyagol, J. Tonannavar, and Jayashree Tonannavar. "Computational and Experimental Studies on Double H-Bonded Zwitterion Dimer Model for L-2-Aminoadipic Acid.". *Asian Journal of Chemistry*, **37**:1431–1448, 2025.
DOI: https://doi.org/10.14233/ajchem.2025.33831.

[53] M. Kotyagol, J. Tonannavar, and Jayashree Tonannavar. "Spectroscopic and Computational Insights into Hydrogen Bonding in (S)-(+)-4-Amino-3-hydroxybutyric acid Dimer". Recent Trends in Applied Physics & Material Science, CRC Press,, 2025.
DOI: https://doi.org/10.1201/9781003684718-74.